Int J Appl Earth Obs Geoinformation xxx (xxxx) xxxx

Contents lists available at ScienceDirect

Int J Appl Earth Obs Geoinformation

journal homepage: www.elsevier.com/locate/jag

Use of local and global maps of forest canopy height and aboveground biomass to enhance local estimates of biomass in miombo woodlands in Tanzania

Erik Næsset[a,*], Ronald E. McRoberts[b], Anssi Pekkarinen[c,1], Sassan Saatchi[d], Maurizio Santoro[e], Øivind D. Trier[f], Eliakimu Zahabu[g], Terje Gobakken[a]

[a] Faculty of Environmental Sciences and Natural Resource Management, Norwegian University of Life Sciences, P.O. Box 5003, NO-1432 Ås, Norway
[b] Department of Forest Resources, University of Minnesota, Saint Paul, MN, 55108, USA
[c] The Food and Agriculture Organization of the United Nations (FAO), 00152 Rome, Italy
[d] NASA-Jet Propulsion Laboratory, California Institute of Technology, Pasadena, CA, 91109, USA
[e] Gamma Remote Sensing, Worbstrasse 225, Gümligen, Switzerland
[f] Norwegian Computing Center, Gaustadalléen 23A, P.O. Box 114, NO-0314 Oslo, Norway
[g] Department of Forest Resources Assessment and Management, Sokoine University of Agriculture, P.O. Box 3013, Chuo Kikuu, Morogoro, United Republic of Tanzania

ARTICLE INFO

Keywords:
Biomass maps
Model-assisted estimation
Systematic map errors
Dry tropical forests

ABSTRACT

Field surveys are often a primary source of aboveground biomass (AGB) data, but plot-based estimates of parameters related to AGB are often not sufficiently precise, particularly not in tropical countries. Remotely sensed data may complement field data and thus help to increase the precision of estimates and circumvent some of the problems with missing sample observations in inaccessible areas. Here, we report the results of a study conducted in a 15,867 km^2 area in the dry miombo woodlands of Tanzania, to quantify the contribution of existing canopy height and biomass maps to improving the precision of canopy height and AGB estimates locally. A local and a global height map and three global biomass maps, and a probability sample of 513 inventory plots were subject to analysis. Model-assisted sampling estimators were used to estimate mean height and AGB across the study area using the original maps and then with the maps calibrated with local inventory plots. Large systematic map errors – positive or negative – were found for all the maps, with systematic errors as great as 60–70 %. After being calibrated locally, the maps contributed substantially to increasing the precision of both mean height and mean AGB estimates, with relative efficiencies (variance of the field-based estimates relative to the variance of the map-assisted estimates) of 1.3–2.7 for the overall estimates. The study, although focused on a relatively small area of dry tropical forests, illustrates the potential strengths and weaknesses of existing global forest height and biomass maps based on remotely sensed data and universal prediction models. Our results suggest that the use of regional or local inventory data for calibration can substantially increase the precision of map-based estimates and their applications in assessing forest carbon stocks for emission reduction programs and policy and financial decisions.

1. Introduction

A regime of economic incentives for reducing emissions from deforestation and forest degradation, and increased sequestration of atmospheric carbon (C) by forest conservation, sustainable management of forests, and enhancement of forest carbon stocks (REDD+) is one way of reducing the increase in atmospheric C. Because payments for C offsets under REDD+ are based on estimates of C stocks and stock changes over time (Herold and Skutsch, 2011; Joseph et al., 2013), a key component and a requirement for successful implementation of REDD+ is a monitoring system that ensures reliable measurement, reporting, and verification of the reduced loss, or net increase of forest C.

Aboveground biomass, which can be converted to carbon with a scaling factor of approximately 0.5, is a variable characterizing the total

DOI of original article: https://doi.org/10.1016/j.jag.2020.102109
* Corresponding author.
E-mail address: erik.naesset@nmbu.no (E. Næsset).
[1] Disclaimer: The views expressed in this publication are those of the author(s) and do not necessarily reflect the views or policies of the Food and Agriculture Organization of the United Nations.

https://doi.org/10.1016/j.jag.2020.102138

mass of trees within an area, and is typically defined in kg per m^2 or Mg per hectare. Aboveground biomass estimates are based on measurements of some biophysical properties of individual trees (e.g. stem diameter) and use of allometric regression models to predict individual tree aboveground biomass – models that have been developed from destructive harvesting of trees of different sizes and types. In the current study, we will use the abbreviation AGB to characterize aboveground biomass per unit area and it is defined in Mg per hectare (Mg ha^{-1}).

Field-based sample surveys – such as national forest inventories (NFIs) have traditionally been used to provide regional and national estimates of AGB and changes in AGB over time satisfying reporting requirements. Thus, field surveys are often a primary source of AGB data, but plot-based estimates of population parameters related to AGB and AGB change are often not sufficiently precise, particularly not in tropical countries where consistent and repeated surveys over time are often lacking.

In most tropical countries in particular, NFIs are either not available or only partially implemented because they are expensive and can be cost-prohibitive or infeasible due to inaccessibility. Remotely sensed data may complement field data and thus help to increase precision and circumvent some of the problems with missing sample observations for inaccessible areas. This is also acknowledged by The Conference of the Parties (COP) to the United Nations Framework Convention on Climate Change by its request to developing countries to "*Use a combination of remote sensing and ground-based forest carbon inventory approaches for estimating* (…) *anthropogenic forest-related greenhouse gas emissions*" (COP Decision 4/CP.15). In the same decision, COP also requests developing countries "*To use the most recent Intergovernmental Panel on Climate Change guidance and guidelines* (…) *as a basis for estimating anthropogenic forest-related greenhouse gas emissions*". In the most recent guidelines for greenhouse gas inventories of the Intergovernmental Panel on Climate Change (IPCC, 2019), a new section on use of biomass maps extends previous guidelines. Clearly, biomass maps and other maps will play an important role in future inventories to estimate AGB and C stocks and changes over time.

Exactly how existing maps should be adopted to estimate biomass in accordance with the most recently adopted IPCC guidance (IPCC, 2019) is yet an open question. Some guidance may be found in the Methods and Guidance Document of the Global Forest Observation Initiative (GFOI, 2016), but technical details are lacking. Some recent and technical examples have been reported though, including the estimation of AGB and carbon stocks adopted in REDD projects in tropical countries such as in the jurisdictional REDD + project in the Democratic Republic of Congo (Anon, 2016). However, regardless of map data and technical solution selected for the estimation, the IPCC specifies two general and guiding principles for greenhouse gas inventories: (1) "neither over- nor underestimates so far as can be judged," and (2) "uncertainties are reduced as far as is practicable" (Penman et al., 2003). From a statistical perspective, satisfaction of the second criterion requires, at minimum, rigorous estimation of variances. In particular, there can be little assurance that uncertainties are reduced until they are first rigorously estimated (McRoberts et al., 2019a).

For the first guideline, the standard for assessing under- or over-estimation may depend on the chosen approach to statistical inference. Two principle modes of inference may be considered. First, if the estimation process entails use of a probability sample of field plots in combination with a map, design-based inference may be adopted for which design-unbiased estimators exploit the information in the map. When design-unbiased estimators are used, it is reasonable to declare compliance with the first IPCC guideline. Use of design-based estimators and existing maps to estimate forest area and biomass in tropical countries was demonstrated for Brazil by McRoberts et al. (2016) and Tanzania by Næsset et al. (2016). Second, if there is no probability sample of field plots, the only viable option is to use the map as the sole source of data and resort to model-based inference. In this case, the mean AGB estimate for the area of interest (AOI) will be the mean of the individual biomass pixel values of the map within the AOI. It has recently been suggested that the true value must be the standard for assessing under- or over-estimation of such model-based estimates (McRoberts et al., 2019a). Since the true value is not known, the result of a comparison of a model-based estimate with a substitute for the true value must be expressed in probabilistic terms such as a confidence interval. McRoberts et al. (2019a) elaborates on various alternatives for using local maps of greater quality as means to provide a substitute for the true value.

Despite potential limitations of AGB maps to support AGB estimation due to issues related to systematic map errors, AGB maps may still be of substantial value to enhance precision of estimates, especially under design-based inference. Numerous studies adopting design-based estimators of variance have shown reductions of estimated variances by factors of two or more when AGB maps or other maps or various types of remotely sensed data have been used as auxiliary data to assist in the estimation. With design-based inference, even maps displaying substantial inherent systematic errors may be used to enhance precision while the unbiasedness of the AGB estimator of the mean is maintained. Of particular relevance for the current study, which was conducted in dry miombo woodlands of Tanzania, is the study by Næsset et al. (2016). They compared design-based estimates of AGB in the miombo woodlands using airborne lidar, interferometric synthetic aperture radar (InSAR) derived from TanDEM-X, RapidEye optical imagery, and global map products of tree cover constructed from Landsat and forest/non-forest constructed from ALOS PALSAR L-band radar imagery as sources of auxiliary data. Even in a case with substantial systematic map errors in tree cover, the map helped reduce the variance of the AGB estimate.

Field plot sizes often differ from the sizes of map pixels, and that tends to reduce the value of a map as a source of auxiliary data in the estimation. Edge effects (overhanging tree crowns) and field plot positioning errors will have similar detrimental effects on the estimation (Næsset et al., 2015). Full geographical correspondence between field plots and map pixels is also often hampered by imperfect alignment. In a practical world, the inventory compiler will have to live with all these imperfections when using a map to enhance biomass estimates. Nevertheless, the map may still be a valuable source of information that can improve estimates at little or no additional cost.

The current study addressed canopy height and biomass estimation in dry tropical miombo woodlands of Tanzania using existing maps. Miombo woodlands are among the most wide-spread vegetation types in eastern, central, and southern Africa, occupying about 9% of the entire African land area (Frost, 1996; White, 1983). Although there is considerable uncertainty, more than 90 % of the total forest land in Tanzania can likely be defined as miombo (Anon, 1998; Abdallah and Monela, 2007; MNRT, 2015). In spite of a fairly rich literature on the use of different types of remotely sensed data to estimate AGB in areas that also include miombo woodlands (e.g. Mitchard et al., 2011; Baccini et al., 2012; Harris et al., 2012; Carreiras et al., 2013; Gizachew et al., 2016; Egberth et al., 2017; Hojas Gascón et al., 2019), only a few (e.g. Næsset et al., 2016; Ene et al., 2016) address the contribution of the remotely sensed data to enhance estimates of AGB for this forest type. To the best of our knowledge there are no studies on the contribution of existing local and global maps to enhancing the estimates in the dry tropics. Further, we are not aware of any studies that have quantified the potential systematic errors in existing maps – errors that will adversely affect IPCC compliance if carried over to AGB estimates.

Due to the increased focus on the use of AGB and canopy height maps in greenhouse gas inventories, the objectives of the current study were fourfold: (1) to quantify the contribution of existing canopy height and AGB maps to improve the precision of local canopy height and AGB estimates, respectively, in miombo woodlands; (2) to compare the relative contributions of a local and a global canopy height map to improving mean local canopy height estimates; (3) to demonstrate how canopy height maps can be used to improve precision of local AGB estimates; and (4) to quantify potential local systematic errors in existing canopy height and biomass maps. In this study, we included two canopy height maps: a local height map produced by Trier et al. (2018) and a global height map produced by

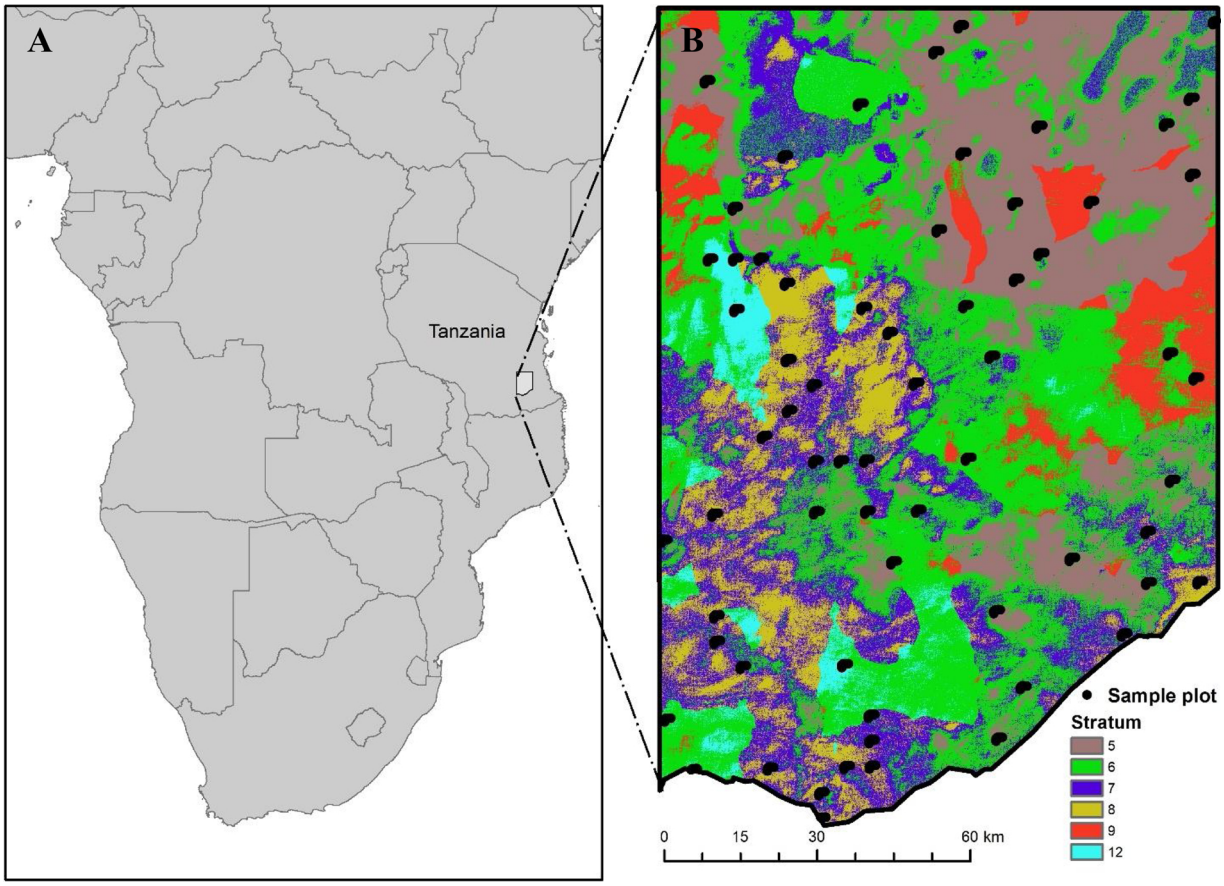

Fig. 1. A: Location of the 15,867 km^2 study area in Liwale district, Tanzania. **B**: Study area with distribution of the NAFORMA sample plots in inverted L-shaped clusters and the stratification. Stratum definitions according to Tomppo et al. (2014): Stratum 5: 0-27 m^3 ha^{-1} volume and 0-10° slope; Stratum 6: 28-61 m^3 ha^{-1} volume and 0-10° slope; Stratum 7: 62-118 m^3 ha^{-1} volume and 0-10° slope; Stratum 8: ≥119 m^3 ha^{-1} volume and 0-10° slope; Stratum 9: 0-27 m^3 ha^{-1} volume and 0-10° slope; Stratum 12: ≥119 m^3 ha^{-1} volume and 0-10° slope.

Yu et al. (2019). Further, we included three global biomass maps: (i) the map produced and published online by the European Space Agency (ESA) GlobBiomass project (Santoro et al., 2018); (ii) the map published online by Global Forest Watch (GFW, 2019); and (iii) the map produced by Yu et al. (2019).

2. Material and methods

2.1. Study area

The study area is located in the Liwale district (9°54'S, 37°38'E) of the Lindi region in southeastern Tanzania and has a total size of 15,867 km^2 (Fig. 1). The climate is characterized by two rain periods per year; a short period from late November to January and a longer period from March to May. Annual precipitation is in the range 600 − 1000 mm. The main dry season is from July to October. The study area contains typical miombo flora of tall trees with shrubs and grasses on the forest floor. The miombo woodlands are characterized by large tree species diversity associated with species such as *Brachystegia sp.*, *Julbernadia sp.*, and *Pterocarpus angolensis*. The cover types within the miombo woodlands comprise areas classified as forest as well other cover types according to the definitions of the recently established national forest inventory of Tanzania – the National Forestry Resources Monitoring and Assessment in Tanzania (NAFORMA; URT, 2010). Photographs from sample plots that illustrate important land cover types are provided in Fig. 2.

2.2. Sampling design

The field sample survey was based on probabilistic sampling principles and used a systematic double-phase stratified cluster sample design. The survey within the AOI was part of the national sample survey of NAFORMA and thus the sampling frame when designing the survey was the entire territory of mainland Tanzania. When designing the NAFORMA sample survey, three separate criteria were used to define the strata: (1) growing stock volume predicted by using Landsat spectral data and an empirical model, (2) slope estimated from a digital elevation model, and (3) estimated time to measure all plots in a single field cluster (Tomppo et al., 2014).

A design-based analysis was chosen for the current study. The fact that NAFORMA was designed as a double-phase stratified survey meant that auxiliary information such as maps and remotely sensed data with full wall-to-wall coverage could not be used in the estimation for population elements other than those in the first phase sample since stratum assignment of all other population elements would be unknown. However, each of the three stratification criteria was represented by a spatially continuous map layer. Thus, posteriori it was possible to construct a spatially continuous stratum map that was consistent with the actual stratification of NAFORMA. After the implementation of NAFORMA and prior to the current study, such a map was constructed by the Food and Agricultural Organization of the United Nations (Anssi Pekkarinen, pers.comm.). We compared the stratum map to the actual stratification of the NAFORMA second-phase sample and found 100 % consistency in stratum assignments within the study area. The stratum map was, therefore, adopted for the current study. That implies that the sampling design could be considered a systematic single-phase stratified design rather than a systematic double-phase stratified design. A single-phase design allowed the full use of wall-to-wall auxiliary information, such as AGB maps, in a

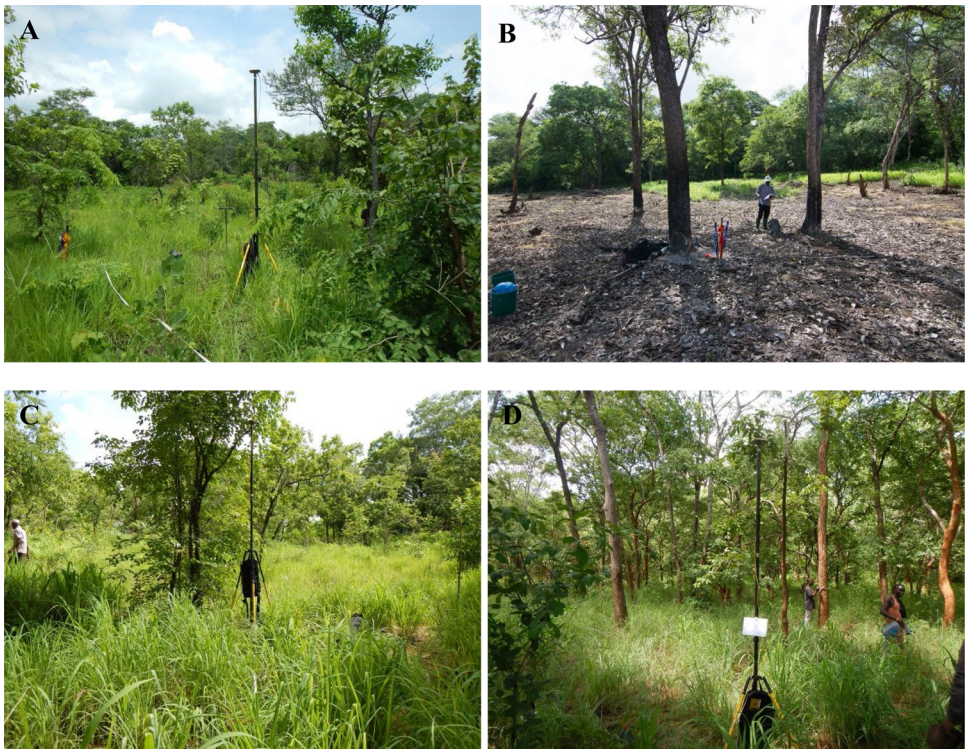

Fig. 2. Examples of sample plots representing different land cover types (definitions in URT, 2010). **A**: Land cover = lowland forest with AGB = 26.0 Mg ha^{-1}. **B**: Land cover = lowland forest with AGB = 48.9 Mg ha^{-1}. **C**: Land cover = closed woodland with AGB = 57.9 Mg ha^{-1} **D**: Land cover = open woodland with AGB = 192.3 Mg ha$^{-1.}$

Table 1
Area, numbers of clusters and plots, observed total aboveground biomass (AGB) and Lorey's mean height (h_L) distributed on strata after re-stratification.

				AGB at plot level (Mg ha^{-1})		h_L at plot level (m)	
Stratum[a]	Area (km^2)	No. of clusters	No. of plots	Range	Mean	Range	Mean
5	3821	15	120	0.0 – 158.2	44.3	0.0 – 18.1	10.2
6	5834	14	112	0.0 – 187.1	50.4	0.0 – 21.1	9.3
7	2903	12	94	0.0 – 270.6	81.8	0.0 – 21.4	11.7
8	1657	16	125	0.0 – 350.3	75.4	0.0 – 21.0	11.0
9	1118	3	24	0.0 – 125.6	37.1	0.0 – 16.5	9.5
12	536	5	38	34.3 – 182.6	85.1	7.0 – 17.4	11.4
All	15,867	65	513	0.0 – 350.3	62.8	0.0 – 21.4	10.5

[a] According to stratum definition in Tomppo et al. (2014).

design-based analysis. The stratum map also defined the elements of the population subject to analysis. Since the map was based partly on Landsat data (the predicted growing stock volume map layer), the 900 m^2 pixels and the Landsat pixel structure defined the population (Sections 2.5,2.6).

The design was previously described as per Tomppo et al. (2014). First, a N-S and E-W oriented grid with 5 km × 5 km distance between the nodes was created. This was the first-phase grid used in the double-phase design employed by NAFORMA. The NW corner of each 5 km × 5 km grid cell served as geographical reference for a potential plot cluster to be measured in field. These locations are designated "cluster reference points". Second, every cluster reference point was then assigned to a stratum, which means that all plots in a cluster were assigned to the same stratum. A stratum-wise systematic selection among the cluster reference points on the 5 km × 5 km grid was then performed to establish the second-phase sample to be measured in field.

In total, NAFORMA defined 18 strata for the entire country. The second-phase sampling intensities varied from 2 to 20, meaning that in the most intensively sampled stratum every second cluster reference point on the 5 km × 5 km grid was selected for field measurements while in the least intensively sampled stratum every 20th cluster reference point was selected. A preliminary analysis of the stratum map and the stratum assignments of the actual field-measured clusters, revealed that 17 strata were present in the AOI, although some of them represented less than 10 ha. The nine smallest strata collectively accounted for only 1.1 % of the total area. Further, there were no field clusters assigned to any of these nine strata. In addition, two of the remaining eight strata had fewer than three assigned clusters. Therefore, we merged each of these 11 strata with one of the six larger strata that had similar sampling intensities and that were similar with respect to stratification criteria #1 – 2 (predicted volume and slope). The result was a stratification and accompanying stratification map with six strata and a total of 65 field clusters that had been re-assigned to the merged strata. Because the 11 merged strata were small and their sampling intensities were similar to those for the strata with which they were merged, the re-stratification only marginally violated the assumptions of stratified sampling with equal inclusion probabilities within a given stratum.

When the 65 field clusters were established in the Liwale district by NAFORMA in 2011, each cluster consisted of 10 field plots (Tomppo et al., 2014). However, when these plots were re-measured in 2012 and 2014 for studies on the use of airborne lidar in dry miombo woodlands (e.g. Mauya et al., 2015; Ene et al., 2017), only eight of the northernmost plots of each cluster were remeasured. Further, some clusters were intersected by the boundary of the study area, leaving seven plots outside the area. Consequently, the total number of plots for this study was 513 (Table 1), i.e., seven plots fewer than 520 plots that would have been expected for 65 clusters of eight plots each. The field

measurements acquired in 2014 were used in the current study (see details below). The unequal numbers of plots per cluster were accommodated in the design-based analysis (see details below).

In each of the 65 clusters, the eight initial plots were located according to a predefined and fixed pattern. Thus, there was no randomization in this part of the design. From the cluster reference point, five plots were established every 250 m in the E-W direction and three plots were established every 250 m in the N-S direction. Thus, the eight plots formed an "L-shaped" cluster (Fig. 1). The plot separation distance of 250 m was chosen to avoid serious spatial correlation in wood volume between adjacent plots and, thus, to increase the amount of unique information contributed by each plot, thereby increasing the efficiency of the inventory. Wood volume is expected to be closely related to AGB. Comprehensive studies of empirical semivariances provided by Tomppo et al. (2014) for the NAFORMA sample survey design showed that the semivariances reached an upper asymptote at a distance of approximately 250 m. Ene et al. (2016) used the very same plots as in the current study and airborne lidar data to construct biomass models. When accounting for the cluster structure of the plots they did not find any significant improvement of the models compared to simpler models (Ene et al., 2016, Appendix A, Supplementary data), which is consistent with the semivariance analysis of Tomppo et al. (2014). It should be noted that any potential spatial correlation among plots within a cluster may reduce the efficiency of the sampling, but it does not compromise the validity of the design-based estimators. The design of the individual clusters as well as the plot size and field protocol were adopted from the NAFORMA program (URT, 2010).

2.3. Field data

The 513 plots were circular with radius of 15 m (707 m^2) and were measured during January-July 2014. Handheld global positioning system (GPS) receivers were used to navigate to the predefined plot centers for which coordinates had been accurately determined by means of differential GPS and global navigation satellite system using 40-channel dual frequency survey grade receivers as field and base receivers during the campaign in 2012. The estimated precision of the planimetric plot coordinates ranged from 0.004 m to 1.407 m with an average of 0.132 m (Ene et al., 2017).

On each plot, the tree measurements were acquired using concentric circular plots to define the diameter limits of trees to be included in the measurements on each part of a plot. The radii of the concentric circles were 2, 5, 10, and 15 m (Tomppo et al., 2014, Fig. 8), and trees with diameter at breast height (*dbh*) greater than 1, 5, 10, and 20 cm, respectively, for the concentric plots of increasing size were measured. Every fifth plot tree was selected as a sample tree for height measurement using Suunto hypsometers. For trees without height measurements tree height was predicted using diameter-height models constructed from the sample trees (Ene et al., 2017). The measured and predicted tree heights were used to calculate Lorey's mean height (basal-area weighted mean height), denoted h_L, on every plot. Plot-level AGB was estimated by summing individual tree biomass predictions using single-tree allometric models of total AGB (Mugasha et al., 2013) with *dbh* and tree height as independent variables. The estimated plot-level AGB was designated" observed total aboveground biomass" (Mg ha^{-1}) even though the estimated values are subject to errors that typically will occur in field values predicted with allometric models and with subsampling of trees to be measured within a plot. In the analysis we treated estimated plot AGB as error free observations because we assumed that the errors were negligible in magnitude compared to sampling variability. AGB on the plots ranged from 0 to 350.3 Mg ha^{-1} with a mean across all plots of 62.8 Mg ha^{-1} (Table 1). h_L on the plots ranged from 0 to 21.4 m with a mean across all plots of 10.5 m.

2.4. Map data

2.4.1. Height maps

2.4.1.1. Local height map. Two height maps were subject to analysis. The first map was produced by Trier et al. (2018) as a local map based on data from the current study area in Tanzania and was provided by the map producer. Based on local airborne lidar campaigns with 25 % of the area covered by parallel lidar strips, a digital surface model with 1 m resolution was constructed with canopy surface defined as the maximum laser echo height in each 1 m^2 cell. The elevation of these cells above the terrain surface was averaged for 30 m × 30 m pixels corresponding to the Landsat-8 pixel structure. These pixel-wise mean height values were the reference canopy heights subject to local canopy height map construction and they were regressed against temporally consistent Landsat-8 spectral data. In the mapping procedure, the regression model and a long times series of available Landsat data combined with a Kalman filter were used to predict annual canopy height. A canopy height map with a nominal date of 2014 was used in the current study.

2.4.1.2. Global height map. The second height map was produced by Yu et al. (2019) using more than seven million lidar waveform-based predictions of forest height from the Geoscience Laser Altimeter Instrument (GLAS) onboard the Ice, Cloud, Land Elevation Satellite (ICESat-1) mission from 2003−2008. The map was produced by using the non-parametric Maximum Entropy algorithm (MaxEnt) and a Bayesian estimation technique using satellite imagery from ALOS PALSAR (2015), Landsat-8 (2015), and the Shuttle Topography Mission (SRTM) data for topography. The map provided estimates of h_L for forests at 1-ha resolution (100 m × 100 m pixel size) globally (Saatchi et al., 2011; Xu et al., 2016). For areas of woodlands and shrubland savanna where the GLAS lidar footprints are sparse and the sample size is insufficient, data from a large number of airborne lidar campaigns distributed across the globe, particularly in tropical regions of all three continents, was included (Lucas et al., 2008; Naidoo et al., 2012; Ene et al., 2017; Xu et al., 2017; Ferraz et al., 2018). A portion of the global map with a nominal date of 2015 was subject to analysis in the current study.

2.4.2. Biomass maps

2.4.2.1. Global Forest Watch map. Three AGB maps were subject to analysis. The first map ("Aboveground live woody biomass density") was produced and published online by Global Forest Watch (GFW, 2019). It was produced by expanding on the methodology detailed in Baccini et al. (2012). Primary data sources were ICESat-1 GLAS lidar waveforms, Landsat-7 ETM + top-of- atmosphere reflectance and tree canopy cover from the global change dataset (Hansen et al., 2013). Random forests was used to model and produce the AGB pixel values valid for the year 2000. The map was resampled to a 30 m × 30 m pixel resolution (GFW, 2019).

Because the field data for the current analysis were collected in 2014, the Global Forest Watch AGB map was updated to 2014 for better temporal consistency by subtracting AGB loss published online by Global Forest Watch. The map product in question ("Tree biomass loss") is given in tons of CO_2 emissions to the atmosphere as a result of biomass loss and is "*based on the colocation of aboveground live woody biomass density values for the year 2000 from Baccini* et al. *(2012) with annual tree cover loss data from 2001 through 2017 from* Hansen et al. (2013). *All of the aboveground carbon is considered to be "committed" emissions to the atmosphere upon clearing. Emissions are "gross" rather than "net" estimates, meaning that information about the fate of land after clearing, and its associated carbon value, is not incorporated*" (GFW, 2019). We converted this loss from CO_2 to biomass by multiplying the CO_2 values by a CO_2-to-biomass conversion factor of 1/44 × 12 × 2. Assuming a linear loss of biomass across time, these biomass values corresponding to the loss over the period 2000–2017 were then multiplied by the factor 14/17 to estimate the loss for the period 2000–2017. The resulting AGB map with a nominal date of 2014 was designated "GFW" and was used in the current study. This updated map ignored potential increase in AGB due to factors such as regrowth and afforestation, and potential decreases in AGB due to partial loss of AGB (e.g. degradation) not accounted for by the Hansen et al. (2013) tree cover

loss data. To assess the magnitude of the losses in the period 2000–2014 that were subtracted from the year 2000 map, and to facilitate comparison with annual losses estimated from independent data sources unique to the area under study, we estimated the losses specifically (see further details below).

2.4.2.2. GlobBiomass map. The second AGB map was produced by the ESA GlobBiomass project (Santoro et al., 2018), is designated "GlobBiomass", and is available online (Globbiomass, 2019). The GlobBiomass map was produced by combining data from radar satellites (ALOS PALSAR and Envisat ASAR) and optical data (Landsat). Additional data from multiple sources including space lidar (ICESat-1 GLAS), field surveys, land cover maps and many other data sources were used for training. A detailed technical description is provided by Quegan et al. (2017). The resulting global AGB map used in the current study had a 1-ha resolution (approximately 100 m × 100 m pixel size at the equator) and was related temporally to the year 2010 (±1 yr).

2.4.2.3. NASA Jet Propulsion Laboratory map. The third biomass map was produced by Yu et al. (2019) at the NASA Jet Propulsion Laboratory and is designated "JPL". The JPL biomass map follows the same methodology as the global forest height map discussed above and covers the global forests, woodlands, and shrublands at the same spatial resolution (1 ha). The map was produced by first predicting the AGB at the footprint level using more than 40 models developed from ground inventory plots and ICESat-1 GLAS-predicted Lorey's height across the global forest types, and then using the MaxEnt algorithm for predicting AGB for every 1-ha pixel. Over tropical dry and wet forests, the AGB predictions were improved compared to earlier versions (Saatchi et al., 2011; Mitchard et al., 2013) by modifying the tropical lidar-AGB models by wood density variations to capture the regional differences in allometry and species composition. The global biomass map used for the current study was related temporally to the year 2015.

2.5. Connecting datasets

The field plots, the stratum map, and the various height and AGB maps had different pixel sizes and shapes, and orientations of their pixel structures.

First, we converted the stratum map reflecting the Landsat pixel orientation and size (30 m × 30 m) defining the population (Sections 2.2 and 2.6) to point data representing the center point of each population element. Second, field plot data (polygons) and these point data were converted to the coordinate system of the various height and AGB maps. Third, height and AGB values from the respective height and AGB maps (Section 2.4) were extracted for each individual plot as the area-weighted means of heights and AGB values for the map pixels that intersected the plot.

Fourth, for the various height and AGB maps, values were extracted for the center point of each population element. These extracted element-wise map values now contained the information from the various height and AGB maps and constituted the data subject to analysis.

2.6. Estimators

We estimated the population parameters mean h_L and mean AGB per hectare and their standard errors for the entire AOI. Since the survey adopted a stratified sampling design, we had to provide corresponding stratum-wise estimates as well, and they were also reported separately. Mean h_L and mean AGB were estimated by using the maps to enhance the estimates. However, estimates using only the field data were provided for the sake of comparison ("benchmark"). We employed the design-based estimators detailed below.

2.6.1. Defining the population

Let $U = \{1, \ldots, k, \ldots, N\}$ be the entire population of N = 17,630,416 population elements in the AOI. The elements were the 900 m^2 pixels of the stratum map corresponding to the Landsat data used to stratify the territory of Tanzania (Section 2.2). Further, the population U was partitioned into M primary sampling units (clusters) denoted $U_1, \ldots, U_i, \ldots, U_M$, each of size N_i. The population U was also divided into H non-overlapping strata denoted $U_1, \ldots, U_h \ldots, U_H$ with known stratum sizes N_h and M_h clusters per stratum where $h = 1, \ldots, H$. In the current study, $H = 6$ after re-stratification (Section 2.2).

2.6.2. Defining the sample

A stratified cluster design was adopted in this study. We now assume that m_h among the M_h clusters in each stratum h were selected by simple random sampling and these stratum-wise samples of clusters were denoted S_h. The sampling was assumed to be carried out independently among strata. The collection of sample units across strata is the overall sample of clusters (denoted S) for the AOI, i.e., the sample of 65 clusters measured in field. For every cluster U_i in S we measured every element in the field, with the exception of a few clusters for which some plots were outside the AOI and therefore were discarded from the analysis. Thus, it was a design assumption that the field plots were selected among the population elements of size 900 m^2, although in reality the plot size was only 707 m^2.

2.6.3. Estimation based on the field sample

Now, let y_k be h_L or AGB of the kth element in the population. When the clusters within a stratum have unequal numbers of plots as in our case, a ratio estimator may be adopted to estimate mean h_L or mean AGB of a stratum (Lohr, 1999, Eq. 5.16). For stratum h, we have

$$\hat{Y}_{\mathrm{FIELD}h} = \frac{1}{\sum_{U_i \in S_h} N_i} \sum_{k \in S_h} y_k \tag{1}$$

where $\sum_{U_i \in S_h} N_i$ is the number of ground plots in stratum h. An estimator for mean h_L or mean AGB across all strata is

$$\hat{Y}_{\mathrm{FIELD}} = \sum_{h \in H} \frac{N_h}{N} \hat{Y}_{\mathrm{FIELD}h} \tag{2}$$

An estimator for the variance of $\hat{Y}_{\mathrm{FIELD}h}$ is (Lohr, 1999, Eq. 5.18)

$$\hat{V}(\hat{Y}_{\mathrm{FIELD}h}) = \left(\frac{m_h}{\sum_{U_i \in S_h} N_i}\right)^2 \frac{1}{m_h(m_h - 1)} \sum_{U_i \in S_h} N_i^2 \left(\frac{1}{N_i} \sum_{k \in U_i} y_k - \hat{Y}_{\mathrm{FIELD}h}\right)^2 \tag{3}$$

where $\frac{m_h}{\sum_{U_i \in S_h} N_i}$ is the inverse of the average number of field plots per cluster in stratum h. Thus, Eq. 3 quantifies the variation between individual cluster means and the overall estimated mean of a stratum. In this estimator and in the subsequent variance estimator we ignored corrections for finite population because the sampling fractions were always very small and a correction would have a negligible influence on the variance estimates. Because a systematic design was adopted within each stratum for the field survey rather than simple random sampling, an overestimation of the variance is a likely consequence of ignoring the systematic design (Särndal et al., 1992).

For the estimate of mean h_L or mean AGB across all strata ($\hat{Y}_{\mathrm{FIELD}}$), the variance was estimated according to

$$\hat{V}(\hat{Y}_{\mathrm{FIELD}}) = \sum_{h \in H} \left(\frac{N_h}{N}\right)^2 \hat{V}(\hat{Y}_{\mathrm{FIELD}h}) \tag{4}$$

2.6.4. Estimation based on the field sample and map data

A commonly adopted method for estimation of the mean for an AOI using a map (or remotely sensed data) is simply to average the pixel values for an existing map or predicted values of h_L or AGB for all population elements (pixels) within the AOI. The predictions are obtained using a technique such as a regression model developed from

ground observations, which in many cases are found only partly within or even completely outside the particular AOI. Such an estimator is known as a synthetic regression estimator (Särndal, 1984; Särndal et al., 1992). As an example, the synthetic regression estimator (SYNT*h*) for mean h_L or mean AGB for all population elements in U_h of a particular stratum h is

$$\hat{Y}_{SYNTh} = \frac{1}{N_h} \sum_{k \in U_h} \hat{y}_k \tag{5}$$

where $\hat{y}_k$ is h_L or AGB in an existing map or predicted according to a regression model for the kth element (pixel) in the population. A synthetic estimator depends purely on the existing map or a model, typically produces estimates with small variances, but may suffer from severe bias (Särndal et al., 1992, p. 411) if the applied map is subject to systematic errors.

However, because the current sample survey was designed according to probability-based principles, we adopted model-assisted estimators (Särndal et al., 1992). Model-assisted estimators use values or predictions for a large sample of population elements – or even all population elements as in the current study, to reduce the variance but rely on observations (e.g. field sample plots) for population elements selected from a probability sample for validity.

For mean h_L or mean AGB, an appropriate model-assisted estimator for stratum h in stratified cluster sampling when the clusters are of unequal size as in the current study, is

$$\hat{Y}_{MAh} = \frac{1}{N_h} \sum_{k \in U_h} \hat{y}_k + \frac{1}{\sum_{U_i \in S_h} N_i} \sum_{k \in S_h} \hat{e}_k \tag{6}$$

where $\hat{e}_k = y_k - \hat{y}_k$. It can be seen that this estimator consists of the synthetic estimator (Eq. 5) with a correction term that adjusts for deviations between the map or model predictions, and the observed values in the sample from the AOI. In cases where a regression model constructed from the sample in stratum h has a sum of model residuals equal to zero, the correction term will also be zero. In cases where the model is transformed in such a way that the residuals do not exactly sum to zero, or the model is constructed from observations outside the sample, or an existing map is used, the correction term will be different from zero. In this study, the correction term was different from zero for some of the analyses because we used existing maps constructed from data external to the AOI. However, when we used local field data to calibrate the existing maps, the correction term was always equal to zero. In fact, estimating and observing the magnitude of the correction term is an appropriate way of assessing systematic error of a map. Thus, in the current study we estimated and reported results for this Horvitz–Thompson-like estimator of bias (Næsset et al., 2015) when an existing map was evaluated. To be explicit, for stratum h this systematic error was estimated as $D_h = \frac{1}{\sum_{U_i \in S_h} N_i} \sum_{k \in S_h} \hat{e}_k$.

A model-assisted estimator for mean h_L or mean AGB across all strata is

$$\hat{Y}_{MA} = \sum_{h \in H} \frac{N_h}{N} \hat{Y}_{MAh} \tag{7}$$

Similarly, systematic error across all strata was estimated according to Eq. 7 by replacing $\hat{Y}_{MAh}$ with D_h.

When estimating the variances of the model-assisted estimates, we have to differentiate between two cases. First is the situation where an existing map or a regression model fitted from sample data partly or totally outside the sample used for estimation is adopted in the model-assisted estimation. In this case, the model-assisted estimator in Eq. 6 is, in fact, the difference estimator (Särndal et al., 1992, p. 221–225). An appropriate variance estimator for stratum h is then

$$\hat{V}(\hat{Y}_{MAh}) = \left(\frac{m_h}{\sum_{U_i \in S_h} N_i}\right)^2 \frac{1}{m_h(m_h - 1)} \sum_{U_i \in S_h} N_i^2 \left(\frac{1}{N_i} \sum_{k \in U_i} \hat{e}_k - \frac{1}{\sum_{U_i \in S_h} N_i} \sum_{k \in S_h} \hat{e}_k\right)^2 \tag{8}$$

where $\frac{m_h}{\sum_{U_i \in S_h} N_i}$, as before, is the inverse of the average number of field plots per cluster in stratum h and $\frac{1}{\sum_{U_i \in S_h} N_i} \sum_{k \in S_h} \hat{e}_k$ is the mean value of $\hat{e}_k$ across all clusters in stratum h. Thus, Eq. 8 quantifies the variation between the individual cluster means of the residuals and the overall mean residual in a stratum.

Second is the situation where a regression model is fitted from the sample that is subsequently used for the estimation. In this case, we have an internal model, and the model-assisted estimator in Eq. 6 is a generalized regression estimator (Särndal et al., 1992, p. 225–230; Särndal, 2011). Since the correction term was always equal to zero, an appropriate variance estimator for stratum h is

$$\hat{V}(\hat{Y}_{MAh}) = \left(\frac{m_h}{\sum_{U_i \in S_h} N_i}\right)^2 \frac{1}{m_h(m_h - 1)} \sum_{U_i \in S_h} N_i^2 \left(\frac{1}{N_i} \sum_{k \in U_i} \hat{e}_k\right)^2 \tag{9}$$

For the estimate of mean h_L or mean AGB across all strata ($\hat{Y}_{MA}$), the variance was estimated according to

$$\hat{V}(\hat{Y}_{MA}) = \sum_{h \in H} \left(\frac{N_h}{N}\right)^2 \hat{V}(\hat{Y}_{MAh}) \tag{10}$$

The standard error (SE) of the estimators $\hat{Y}_{FIELDh}$, $\hat{Y}_{FIELD}$, $\hat{Y}_{MAh}$, and $\hat{Y}_{MA}$ were estimated as the square root of the respective variances.

2.7. Regression model construction

In model-assisted estimation, locally constructed regression models can be used, first, to calibrate height and AGB maps locally prior to use of the calibrated maps for height and AGB estimation, respectively, and second to convert height maps to locally calibrated AGB maps that subsequently can be used to estimate AGB.

Thus, in the current study we constructed three sets of regression models. The form of these assisting models was defined a priori and was as simple and generic as possible.

First, for the local and global height maps, simple linear regression models of the form

$$h_L = \beta_0 + \beta_1 H + \varepsilon \tag{11}$$

were estimated with the ordinary least squares method (OLS), where h_L is Lorey's mean height estimated for each plot according to the field measurements. h_L was assumed to be estimated without error. H is the height value for the plots extracted from the local and global height maps, respectively, and ε is a normally distributed error term. It should be noted that a simple model ignoring the cluster structure of the plots was adopted in Eq. 11 and in the subsequent models. However, we have no evidence of any spatial correlation among plots within clusters (cf. Tomppo et al., 2014 and Ene et al., 2016), and even if such correlations would be present in the data and thus violating the assumptions in the model construction of independent observations, the estimators adopted in the current study would still be approximately unbiased (Särndal et al., 1992, p. 239).

Second, for the global AGB maps, simple linear regression models of the form

$$AGB = \beta_0 + \beta_1 AGB_{map} + \varepsilon \tag{12}$$

were estimated with OLS. Here, AGB is the field value for each plot and AGB_{map} is the AGB map value for the plots extracted from the three global AGB maps.

Third, for the local and global height maps, simple linear regression models of the form

$$AGB = \beta_0 + \beta_1 H + \varepsilon \quad (13)$$

were estimated with OLS to convert height to AGB. For all the three sets of models (Eqs. 11–13), separate models were constructed for each of the six strata.

After the models were constructed, they were used to produce locally calibrated prediction maps that were applied in the subsequent model-assisted estimation.

2.8. Estimation

2.8.1. Estimation of mean height

Mean estimates of h_L were calculated using only the field sample by applying the stratum-wise cluster sampling estimator (Eq. 1). The SE was also calculated for each stratum (Eq. 3) as were mean h_L estimates across all strata (Eq. 2) and corresponding SE estimates (Eq. 4).

Mean h_L was also estimated stratum-wise by using the local and global height maps in their original form using the model-assisted estimator (Eq. 6) and across all strata using Eq. 7. Corresponding estimates of SE were also calculated (Eqs. 8 and 10). Stratum-wise systematic errors (D_h) and systematic errors across all strata were estimated for the original height maps, and the levels of significance based on two-sided t-tests ($t = D_h/\mathrm{SE}$) with $\sum_{U_i \in S_h} (N_i - 1)$ degrees of freedom were reported.

Finally, mean h_L was estimated stratum-wise using the locally calibrated prediction maps of height produced by the prediction model in Eq. 11 and the model-assisted estimator (Eq. 6) and subsequently across all strata using Eq. 7. Corresponding estimates of SE were calculated (Eqs. 9 and 10).

For all model-assisted estimates, we quantified the gain in precision of the mean h_L estimates of using the maps to assist in the estimation and to compare the contribution of the maps depending on whether they were locally calibrated or not. We used relative efficiency (RE) as a measure of the magnitude of the estimated variance of a model-assisted estimate of mean h_L relative to a pure field-based estimate. It should be noted that the sample sizes always were similar for the pair of variances compared by RE. If $\hat{V}_{\mathrm{map}}$ denotes the estimated variance for a particular model-assisted estimate and $\hat{V}_{\mathrm{field}}$ denotes the estimated variance of a field-based estimate, then RE was calculated as

$$\mathrm{RE} = \frac{\hat{V}_{\mathrm{field}}}{\hat{V}_{\mathrm{map}}} \quad (14)$$

As an example, a value of RE of 1.8 means that the efficiency of the model-assisted estimate is 80 % greater than the field-based estimate, which implies that an 80 % larger sample size would be required for a field-based estimate to produce the same variance as the model-assisted estimate, assuming a constant cluster size.

2.8.2. Estimation of mean aboveground biomass

As for h_L, we first estimated the mean AGB stratum-wise (Eq. 1) and across all strata (Eq. 2) using only the field sample. Subsequently we calculated corresponding SE estimates (Eqs. 3 and 4).

2.8.2.1. Estimation of mean aboveground biomass using biomass maps. Mean AGB was then estimated stratum-wise and across all strata for each of the three global AGB maps in their original form using the model-assisted estimators (Eqs. 6 and 7). SE estimates were also calculated (Eqs. 8 and 10). Stratum-wise systematic map errors of the original maps (D_h) and across all strata were estimated and their statistical significance assessed according to the t-test detailed above.

Finally, mean AGB was estimated stratum-wise by using the three locally calibrated prediction maps of AGB produced by the prediction model in Eq. 12 and the model-assisted estimator (Eq. 6) and subsequently across all strata according to Eq. 7. Corresponding estimates of SE were calculated (Eqs. 9 and 10). RE was calculated for all the model-assisted estimates using Eq. 14.

A specific challenge was associated with the GFW map. As noted above, the GFW map had a nominal date of 2000, and we corrected for losses in the period 2000–2014, see details in Section 2.4.2. Since the model-assisted estimates using field sample data from 2014 will force any estimate – regardless of the nominal year of the map, to be an estimate as per 2014, a potentially incorrect update of the 2000 map will influence the precision of the estimate, not the bias properties of the estimator. Further, incorrect updates will influence the estimated bias of the updated map. We did not have any field data for year 2000 that would have enabled model-assisted estimate of change. Nevertheless, to get an indication of the magnitude of the mean AGB loss that was subtracted from the year 2000 map, we estimated the loss using a synthetic estimator as in Eq. 5, with the only difference that strata were ignored since all elements were accounted for in the synthetic loss estimate. For clarity it should be noted that $\hat{y}_k$ in Eq. 5 was the map-based loss for element (pixel) k according to Hansen et al. (2013), see details in Section 2.4.2.

2.8.2.2. Estimation of mean aboveground biomass using height maps. Mean AGB was estimated stratum-wise using the locally calibrated prediction maps of AGB produced from the local and global height maps, respectively, according to the prediction model in Eq. 13 and the model-assisted estimator (Eq. 6) and subsequently across all strata according to Eq. 7. Corresponding estimates of SE were calculated (Eqs. 9 and 10) as was RE for the model-assisted estimates using Eq. 14.

3. Results and discussion

3.1. Regression models

The 42 regression models that were constructed to calibrate the local and global height maps to local plot data (Eq.11), to calibrate the global AGB maps to local plot data (Eq. 12) and to construct local AGB maps from the local and global height maps (Eq. 13) are presented in Appendix A.

For 33 of the 42 models an extra sum of squares F-test showed that inclusion of the respective explanatory map variables in the models resulted in better fit of the models to the data (Table A1). It was a general finding across all maps for h_L as well as AGB that inclusion of the explanatory variable did not result in a statistically significantly better fit of the model to the data for stratum 12. According to the field data, stratum 12 had the second largest mean h_L (11.4 m; Table 1) and the largest mean AGB (85.1 Mg ha^{-1}). At the same time, the sample size in stratum 12 was the second smallest among the strata (38 plots). Thus, likely reasons for statistically nonsignificant improvement of the models by including the respective map variables in the models can be the small sample size, which will result in larger uncertainty of the estimates, and lower sensitivity of the remotely sensed data used to produce the maps to capture variations in height and biomass for larger tree heights and greater biomass. As is evident from the models in Table A1, the local calibration in stratum 12 therefore largely entailed assignment of a fixed value (the constant term of the models) for all population elements of the stratum, namely values that were not far from the mean value of the field plots. In stratum 12, R^2 was ≤ 0.03 for all models, while for the other strata the models displayed R^2 values in the range < 0.01 to 0.42.

3.2. Estimation of mean height

The estimated mean h_L ranged between 9.3 m and 11.7 m for the respective strata using only the field data (Table 2). Standard errors ranged between 0.45 m and 1.04 m. For the AOI, the overall field-based estimate was 10.2 m (SE = 0.32 m).

When the uncalibrated local and global height maps were used to

Table 2
Estimated mean of Lorey's mean height, systematic error (D_h), and standard error (SE) (m).

			Model-assisted									
			Local height map[a]					Global height map[b]				
	Field-based		Original form			Calibrated		Original form			Calibrated	
Stratum	Mean	SE	Mean	SE	D_h	Mean	SE	Mean	SE	D_h	Mean	SE
5	10.2	0.45	10.0	0.38	5.8***	10.1	0.40	8.9	0.48	4.1***	9.8	0.33
6	9.3	0.71	9.1	0.65	3.7***	9.2	0.62	9.4	1.15	1.4ns	9.3	0.60
7	11.7	0.59	12.8	0.50	6.7***	12.6	0.49	12.5	0.87	2.7**	11.9	0.50
8	11.0	0.69	11.4	0.62	4.5***	11.3	0.62	11.6	0.62	−0.1ns	11.2	0.55
9	9.5	1.04	9.6	1.05	5.7***	9.5	1.04	10.9	0.37	6.6***	10.8	0.38
12	11.4	0.88	11.6	1.16	3.6**	11.3	0.85	11.8	1.31	−1.3ns	11.3	0.80
All	10.2	0.32	10.3	0.29	5.0***	10.3	0.28	10.2	0.47	2.4***	10.3	0.26

Level of significance: ns: not significant ($p > 0.05$); *: $p < 0.05$; **: $p < 0.01$; ***: $p < 0.001$.
[a] Trier et al. (2018).
[b] Yu et al. (2019).

assist in the estimation, similar estimates of mean h_L were obtained. When the local height map was used, the stratum-wise mean h_L estimates ranged between 9.1 m and 12.8 m, whereas use of the global height map resulted in estimates of 8.9–12.5 m. The overall estimates across all strata were 10.3 m and 10.2 m, respectively, for the two maps. None of the model-assisted estimates differed significantly from the pure field-based estimates. The uncertainties tended to be smaller for the uncalibrated model-assisted estimates for the local map than for the pure field-based estimates, with stratum-wise SE of 0.38–1.16 m and overall SE of 0.29 for the local map. For the global map, however, the uncertainties tended to be greater for the uncalibrated model-assisted estimates than for the pure field-based estimates, with stratum-wise SE of 0.37–1.31 m and overall SE of 0.47 for the global map. This resulted in RE values ranging from 0.6 to 1.4 for the local map, with RE equal to 1.2 across all strata, and similarly RE of 0.4–7.9 and 0.5 across all strata for the global map (Table 3).

The systematic errors were generally large. D_h ranged between 3.6 m ($p < 0.01$) and 6.7 m ($p < 0.001$) when using the local map and between -1.3 m ($p > 0.05$) and 6.6 m ($p < 0.001$) when using the global map. Overall, across all strata, the respective systematic errors for the two maps were 5.0 m ($p < 0.001$) and 2.4 m ($p < 0.001$). Thus, in the most extreme cases the systematic errors were as great as approximately 60 % of the estimated mean for the local map and as great as 70 % for the global map. It should be noted that the local map always displayed positive systematic errors, meaning that the synthetic estimates (i.e., pure map-based estimates; Eq. 5) always underestimated the stratum-wise means on the field plots, while the global height map for some strata displayed an overestimation, although the overestimation was always non-significant in the statistical sense (Table 2).

A small fraction of the AOI is displayed in the maps in Fig. 3. For this particular area, it is evident that the local map tended to have smaller height values over the landscape than the global map (Figs. 3A and 3C).

Table 3
Relative efficiency for mean estimates of Lorey's mean height.

	Local height map[a]		Global height map[b]	
Stratum	Original form	Calibrated	Original form	Calibrated
5	1.4	1.3	0.9	1.9
6	1.2	1.3	0.4	1.4
7	1.4	1.5	0.5	1.4
8	1.2	1.2	1.2	1.6
9	1.0	1.0	7.9	7.5
12	0.6	1.1	0.5	1.3
All	1.2	1.3	0.5	1.5

[a] Trier et al. (2018).
[b] Yu et al. (2019).

At least two important features of the map construction procedures of the two respective maps may explain differences in systematic errors. First, the local map did not adopt a canopy height definition that was specifically related to h_L. Instead, the local map used canopy height as extracted from local airborne lidar data according to a specific data processing routine to define height, whereas the global map used h_L as the definition of height. Second, although the local map used local data for map construction while the global map by "global" alludes to a global calibration of models used to construct the map, even the global map used local data (Section 2.4.1). In fact, when constructing the global map, the very same field plots as used in the current study with the same plot-wise h_L values were used as part of the dataset used for model training and map construction. Thus, access to local data may have reduced potential local systematic map errors in the global map that otherwise may occur in areas where data for model calibration and map construction may be sparse or non-existing.

When the maps were calibrated using locally constructed regression models, the model-assisted mean estimates of h_L remained essentially the same as with use of uncalibrated maps (Table 2) whereas the precision increased substantially for the global map but not for the local map. For the local map, the stratum-wise SE estimates ranged from 0.40 m to 1.04 m while for the global map SE ranged from 0.33 m to 0.80 m. The estimates of SE for mean h_L across all strata were 0.28 m and 0.26 m for the local and global maps, respectively. Thus, RE of 1.3 and 1.5 were obtained for the overall estimates when using the two calibrated maps. Calibration of the maps with local regression models resulted in maps that were free from systematic errors, as is illustrated in Fig. 3B and D.

As an overall assessment of the results, estimates of mean height demonstrate that local systematic errors of local as well as global maps can be substantial, even when local data are part of the data used to train and construct the maps. Even when the map is entirely local, substantial systematic errors can occur when there are inconsistencies between the definitions of height in the field survey used as reference and in the data used to train and construct the map. When uncalibrated maps are used to assist in the estimation, the model-assisted estimates may display smaller precision than the pure field-based estimates, as was evident for the global map, while when the very same maps are calibrated locally, they can contribute to substantial improvements in precision over pure field-based estimates. Local calibration therefore seems to be essential, at least in the current case. We did not see any benefits of using an entirely local map over a global map as long as the definitions of height were not harmonized. This observation may, however, be somewhat confounded by the fact that even the global map in our particular case had access to – and did use, local data in

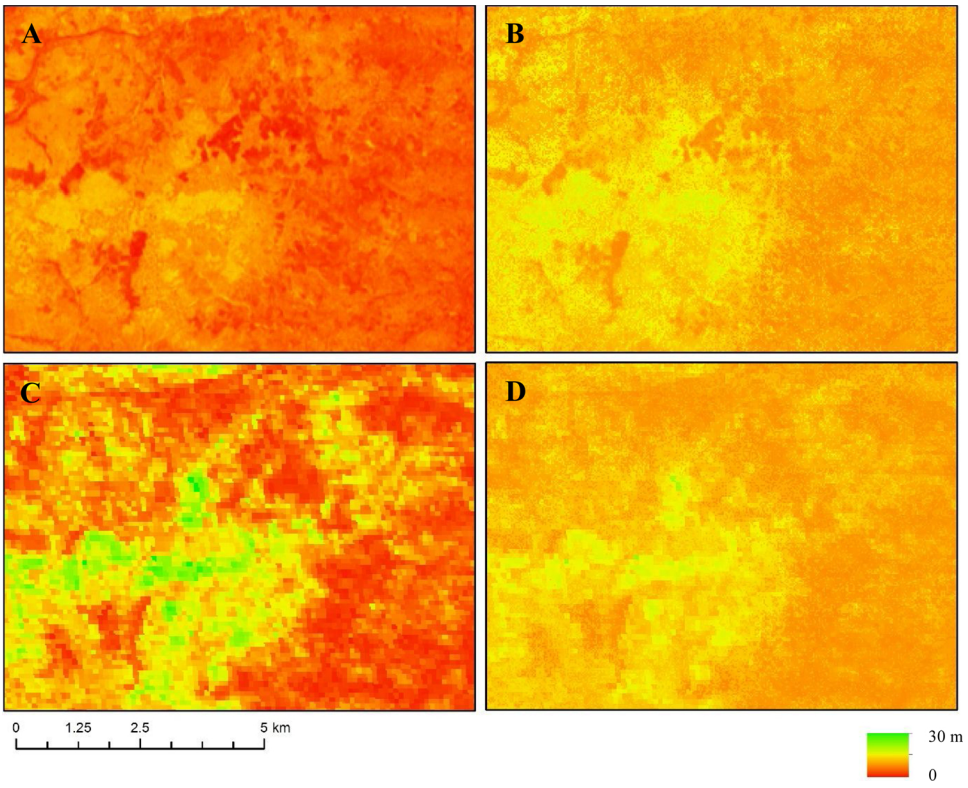

Fig. 3. Height maps for a small region of the study area. **A**: Local height map produced by Trier et al. (2018). **B**: Local height map calibrated according to prediction model in Eq. 11 (Table A1). **C**: Global height map produced by Yu et al. (2019). **D**: Global height map calibrated according to prediction model in Eq. 11 (Table A1). Map sizes are 7.0 km × 9.5 km with center at 9°55′S, 37°52′E.

construction of the global map.

3.3. Estimation of mean aboveground biomass from biomass maps

The field-based estimates of mean AGB ranged between 37.1 Mg ha^{-1} and 85.1 Mg ha^{-1} for the respective strata with SE ranging from 4.42 Mg ha^{-1} to 12.48 Mg ha^{-1} (Table 4). The overall stratified mean AGB estimate for the entire AOI was 57.5 Mg ha^{-1} (SE = 4.00 Mg ha^{-1}). Ene et al. (2017) estimated mean AGB for the same AOI by using the same sample of field plots from the same year (2014) and reported a mean stratified estimate of 58.6 Mg ha^{-1}, well in line with the current estimate. However, their estimate of SE was 5.03 Mg ha^{-1}, 26 % greater than the current estimate. Ene et al. (2017) assumed a double-phase stratified design as opposed to a single-phase stratified design in the current study because they did not have access to the spatially continuous stratum map. Thus, this design effect was substantial and the stratum map evidently has a great value, also in monetary terms, as it represents savings by about 42 % in terms of a reduced need for field plots without having to relax the precision requirements under the simplifying assumption that all clusters are equally large.

The model-assisted stratum-wise estimates of mean AGB using the global biomass maps in their original form were in the ranges 39.7-85.5 Mg ha^{-1}, 39.4-87.6 Mg ha^{-1}, and 31.4-89.6 Mg ha^{-1}, for the GFW, GlobBiomass, and JPL biomass maps, respectively (Table 4). The overall stratified mean AGB estimates were similar among the maps; 59.0 Mg ha^{-1}, 58.3 Mg ha^{-1}, and 57.8 Mg ha^{-1}, respectively. The SE tended to be smaller across all strata and maps compared to the pure field-based estimates, with stratum-wise RE in the ranges of 0.2–3.8, 0.9–3.9, and 0.6–6.4, for the three respective maps (Table 5). For 14 of the 18 stratum and map combinations RE was greater than 1.0. The SE of the overall

Table 4
Estimated mean biomass, systematic error (D_h), and standard error (SE) based on biomass maps (Mg ha^{-1}).

			Model-assisted														
			GFW biomass map[a]					GlobBiomass map[b]					JPL biomass map[c]				
	Field-based		Original form			Calibrated		Original form			Calibrated		Original form			Calibrated	
Stratum	Mean	SE	Mean	SE	D_h	Mean	SE	Mean	SE	D_h	Mean	SE	Mean	SE	D_h	Mean	SE
5	44.3	4.42	42.4	4.17	−23.3***	43.7	3.74	39.4	2.74	13.3***	40.7	2.80	31.4	5.03	−8.9ns	40.0	3.27
6	50.4	8.39	52.8	6.48	−33.2***	52.0	5.18	54.0	4.62	12.6**	53.8	4.65	50.8	8.46	−20.9*	50.6	4.82
7	81.8	10.87	84.2	6.66	−12.5ns	84.4	6.63	81.0	8.18	29.5***	80.8	8.17	89.6	7.49	−1.1ns	87.4	7.20
8	75.4	7.50	78.8	5.76	−29.6***	76.9	5.92	79.2	5.33	17.9**	79.6	5.17	82.7	4.90	−28.8***	78.7	5.11
9	37.1	12.48	39.7	6.38	−25.5***	31.2	9.62	41.5	6.35	19.1**	45.3	2.40	50.3	4.94	15.4**	51.8	4.31
12	85.1	6.71	85.5	13.67	−37.7**	85.2	6.96	87.6	7.09	23.5**	85.2	6.70	88.3	8.46	−36.7***	85.3	6.60
All	57.5	4.00	59.0	3.00	−26.3***	58.7	2.61	58.3	2.47	17.2***	58.7	2.44	57.8	3.67	−13.2***	59.0	2.43

Level of significance: ns: not significant ($p > 0.05$); *: $p < 0.05$; **: $p < 0.01$; ***: $p < 0.001$.
[a] GFW (2019).
[b] Santoro et al. (2018).
[c] Yu et al. (2019).

Table 5
Relative efficiency for estimates of mean biomass.

	GFW biomass map[a]		GlobBiomass map[b]		JPL biomass map[c]	
Stratum	Original form	Calibrated	Original form	Calibrated	Original form	Calibrated
5	1.1	1.4	2.6	2.5	0.8	1.8
6	1.7	2.6	3.3	3.3	1.0	3.0
7	2.7	2.7	1.8	1.8	2.1	2.3
8	1.7	1.6	2.0	2.1	2.3	2.2
9	3.8	1.7	3.9	28.6	6.4	8.4
12	0.2	0.9	0.9	1.0	0.6	1.0
All	1.8	2.3	2.6	2.7	1.2	2.7

[a] GFW (2019).
[b] Santoro et al. (2018).
[c] Yu et al. (2019).

stratified mean AGB estimates varied somewhat between the three maps with SE of 3.00 Mg ha^{-1}, 2.47 Mg ha^{-1}, and 3.67 Mg ha^{-1} for the GFW, GlobBiomass, and JPL maps, respectively. These SE estimates correspond to RE of 1.8, 2.6, and 1.2, respectively. Thus, in their original form all three AGB maps resulted in greater precision when used as assisting data in the estimation as compared to using only the field data in the estimation. This suggests that there is a small, but positive contribution of the global biomass maps in their original form to enhance the estimates.

As was evident for height estimation with support from local and global height maps, the mean stratum-wise model-assisted estimates of AGB after calibration with local regression models were generally well in line with the mean estimates using the maps in their original form, although a few large differences occurred such as in stratum 5 for the JPL map where the two estimates were 31.4 Mg ha^{-1} and 40.0 Mg ha^{-1}, respectively (Table 4). However, these estimates were not significantly different in the statistical sense. The overall stratified estimates of mean AGB when using calibrated maps were also similar to the estimates obtained by using maps in their original form.

For two of the maps there was a substantial gain in precision by using locally calibrated maps rather than original maps. For the overall AGB estimates, SE was reduced from 3.00 Mg ha^{-1} to 2.61 Mg ha^{-1} for the GFW map and from 3.67 Mg ha^{-1} to 2.43 4 Mg ha^{-1} for the JPL map. For the GlobBiomass map, there was no gain in precision (2.47 Mg ha^{-1} versus 2.44 Mg ha^{-1}). RE was equal to or greater than 1.0 for 17 of the 18 stratum and map combinations. For the overall mean AGB estimates, RE was 2.3, 2.7, and 2.7 for the GFW, GlobBiomass, and JPL maps, respectively (Table 5). Thus, all maps in locally calibrated form contributed substantially to improving precision of estimates, with potential for large financial savings in future field-based inventories, as discussed above. It is also noteworthy that the two maps that contributed to the greatest gain in precision – the GlobBiomass and JPL maps, both have a primary spatial resolution of approximately 1 ha while the field plots had a size of just approximately 0.07 ha (707 m^2), whereas the GFW map with a primary resolution of 0.09 ha, very similar to the ground plots, resulted in the least gain in precision. Thus, the greater spatial detail and the seemingly greater information content of the GFW map as illustrated in Fig. 4 in original as well as calibrated form compared to the coarser-resolution GlobBiomass and JPL maps (Fig. 4) do not necessarily contribute to greater utility in the form of greater precision of the estimates. Greater spatial detail and visual similarities between different maps are sometimes confused with the usefulness and value of a map. The current analysis demonstrated that fine spatial resolution is not necessarily a guarantee for a useful map content.

Different sensors and procedures were used to produce the respective maps, which in part may explain the differences. Nevertheless, this also illustrates that discrepancies in field plot sizes and sizes of the primary map units (pixels) are not necessarily a hindrance to useful utilization of such field and map data by combining them in modeling and estimation, even in relatively fragmented forests such as the miombo woodlands of the current analysis. There is probably even more to be gained in terms of improved precision of estimates by a greater correspondence in spatial resolution and alignment between plots and map pixels. It is, however, important to balance the technical gains in terms of precision and the economic impacts in terms of a need for potentially smaller sample sizes on one hand and larger and more expensive field plots on the other to find an appropriate balance between field plot sample sizes, plot sizes, and map pixel sizes. Unfortunately, there is little evidence in the literature regarding the costs and precision of using different plot sizes in combination with maps of different resolutions in forests in general, and in dry tropical woodlands more specifically. In fact, to the best of our knowledge, the only evidence from dry tropical forests of the contribution of global maps or other remotely sensed data to improve precision of biomass estimates beyond what one may obtain by using field data only is the study by Næsset et al. (2016). Their study was conducted in a small subregion of the Liwale district with size 366 km^2. Field data were collected according to a probabilistic, non-stratified design with greater sampling intensity than in the current study but with the same field plot size (707 m^2). For model-assisted estimates of mean AGB, they reported RE of using local biomass prediction maps of 2.8, 3.3., and 3.6 when InSAR data from TanDEM-X, RapidEye optical imagery, and airborne lidar data, respectively, were used to produce the maps. Furthermore, locally calibrated Landsat and ALOS PALSAR maps resulted in RE of 1.3 − 1.4. The current findings based on global AGB maps seem to be well in line with these previous results, although the global AGB maps in general seem to carry more information for AGB estimation than the products derived from Landsat (tree cover; Hansen et al., 2013) and ALOS PALSAR (HH backscatter; Shimada et al., 2014).

All three analyzed AGB maps exhibited large systematic errors. For the GFW map, D_h was negative for all strata, with values ranging from -12.5 Mg ha^{-1} ($p > 0.05$) to -37.7 Mg ha^{-1} ($p < 0.01$) (Table 4). In the most extreme case, the systematic error was approximately 65 % of the estimated mean AGB. The systematic error across all strata was -26.3 ($p < 0.001$). Pure map-based (synthetic) estimates would therefore have greatly overestimated the AGB. As noted in Section 2.4.2, however, we corrected the primary GFW AGB map from year 2000 for losses in the period 2000–2014. The correction accounted for loss in tree cover, which may not be sensitive to smaller losses caused by degradation. Gains in AGB were also ignored. An assessment of the magnitude of the correction showed that the total correction (synthetic estimate) was 4.36 Mg ha^{-1} for the whole period, which corresponds to an average annual loss of 0.31 Mg ha^{-1}. For the same AOI, Ene et al. (2017) had repeated measurements on the same sample of field plots in 2012 and 2014, which represents the last two years of the period for which we corrected the year 2000 GFW map. Ene et al. (2017) provided different change estimates. For an estimate based on a sample of repeated airborne lidar data covering approximately 25 % of the entire AOI, they provided a model-based estimate of annual net loss for the two-year period of 0.17 Mg ha^{-1}. Losses and gains in AGB may vary from year to

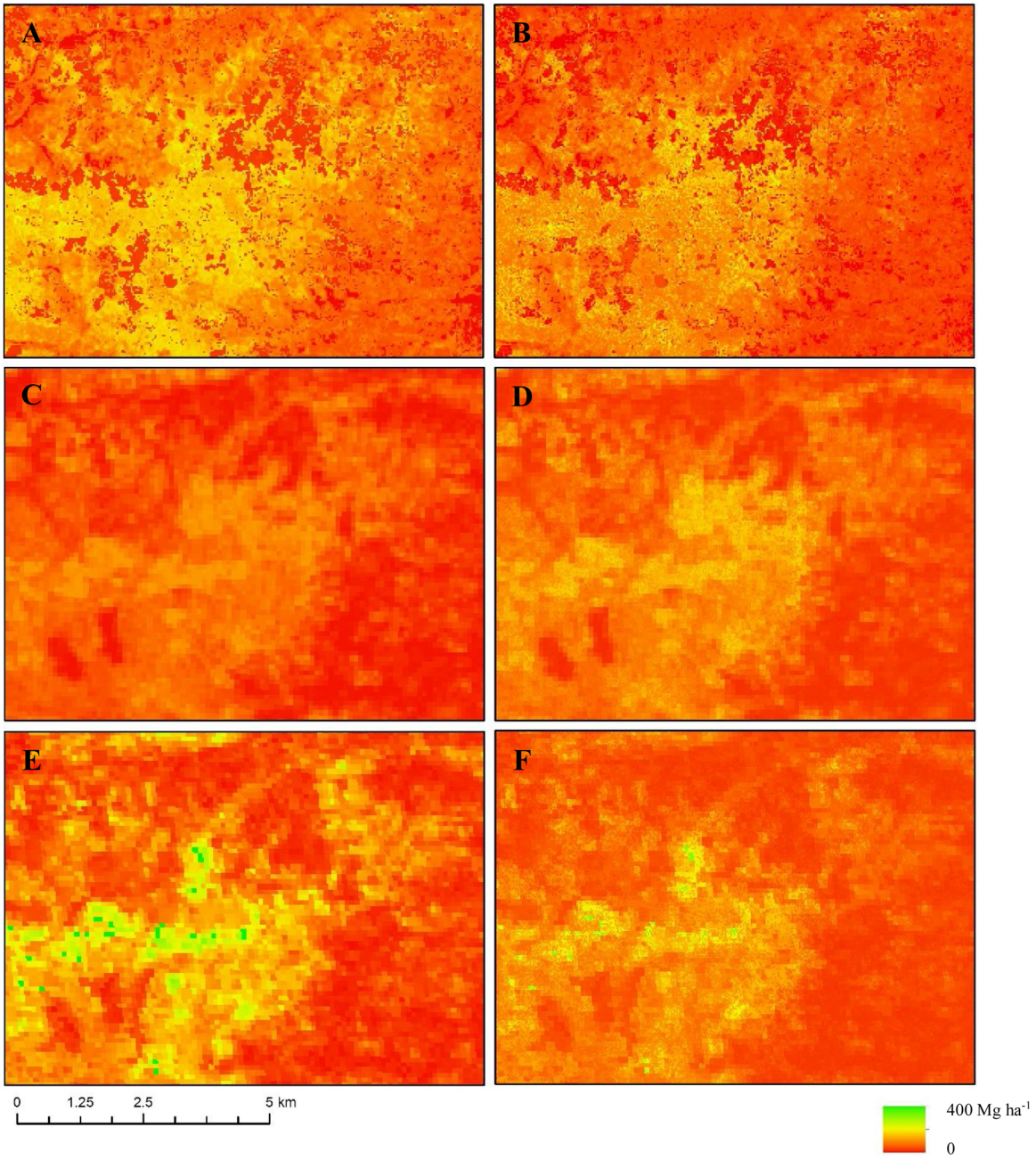

Fig. 4. Biomass maps for a small region of the study area. **A**: GFW biomass map (GFW, 2019). **B**: GFW biomass map calibrated with local plot data according to Eq. 12 (Table A1). **C**: GlobBiomass map produced by Santoro et al. (2018). **D**: GlobBiomass map calibrated with local plot data according to Eq. 12 (Table A1). **E**: JPL biomass map produced by Yu et al. (2019). **F**: JPL biomass map calibrated with local plot data according to Eq. 12 (Table A1). Map sizes are 7.0 km × 9.5 km with center at 9°55′S, 37°52′E.

year. Even if the annual loss applied to correct the year 2000 GFW map was almost twice as large as the annual loss estimated by Ene et al. (2017), the difference over the entire 14-yr period would not be greater than approximately 2 Mg ha^{-1}. Thus, the large systematic errors of the year 2014 GFW map was most likely only marginally influenced by a potentially inaccurate correction of the year 2000 map.

As opposed to a negative systematic error for the GFW map, the GlobBiomass map displayed positive systematic errors in all strata. D_h ranged from 12.6 Mg ha^{-1} ($p < 0.01$) to 29.5 Mg ha^{-1} ($p < 0.001$) and the estimates of systematic error were statistically significant for all the six strata. The largest error in any individual stratum was approximately 45 % of the mean AGB estimate. The systematic error across all strata was 17.2 Mg ha^{-1} ($p < 0.001$). Positive systematic errors imply that an estimate of AGB from the map alone would have resulted in a large underestimation of the AGB.

For the JPL AGB map, there was a mix of positive and negative systematic errors, which was not very surprising, given the use of the local field data as part of the dataset adopted in the map construction. The systematic errors were still large in some of the strata, and D_h ranged from -36.7 Mg ha^{-1} ($p < 0.001$) to 15.4 Mg ha^{-1} ($p < 0.01$), with statistically significant systematic error estimates for four of the strata. The largest error in any individual stratum was approximately 40 % of the estimated mean AGB. The systematic error across all strata was -13.2 ($p < 0.001$).

The large over- and underestimation that were inherent in the respective maps are well illustrated in the maps in Fig. 4. The generally greater AGB values in the original GFW map (Fig. 4A) compared to the smaller values in the GlobBiomass map (Fig. 4C) are clearly visible.

Furthermore, Fig. 4B, D and F, which are the locally calibrated prediction maps of GFW, GlobBiomass, and JPL, show a very pronounced effect of the calibration and that they all appear more similar in AGB levels after the calibration.

Altogether, the analysis of the three global AGB maps shows that they all display systematic errors – errors so large in magnitude that the maps have little value as the sole source of information in the AOI dominated by dry miombo woodlands. The fact that the systematic errors are both positive and negative makes it difficult to use a map as long as the user is unaware of the magnitude and direction of the systematic error of a particular map considered for use. It is, however, striking to see the great potentials for gain in precision when using the maps in calibrated form as assisting data in the estimation. In fact, the maps have great value in financial terms if used in an appropriate way as they may help reduce field sample sizes and save money without having to relax the precision requirements of the estimates. It should also be noted that a fine spatial resolution of a map is no guarantee for greater utility of the map. On the contrary, a coarse-resolution map may sometimes carry more useful information, as demonstrated here. Substantial differences in field plot sizes and map pixel sizes do not necessarily mean that their combined application in modeling and estimation is irrelevant, at least not so when the sample sizes are fairly large.

3.4. Estimation of mean aboveground biomass from height maps

The model-assisted stratum-wise estimates of mean AGB using AGB prediction maps based on local calibration of the local and global height maps (Eq. 13) as auxiliary data ranged between 37.8 Mg ha^{-1} and 100.8 Mg ha^{-1} for the local height map and between 39.6 Mg ha^{-1} and 87.6 Mg ha^{-1} for the global height map (Table 6). With the exception of the estimates for stratum 7 using the local height map (100.8 Mg ha^{-1}) and stratum 9 using the global height map (50.7 Mg ha^{-1}) these estimates were similar to those reported in Section 3.3. However, neither of these estimates differed significantly from the corresponding field-based estimates (81.8 Mg ha^{-1} and 37.1 Mg ha^{-1}).

Stratum-wise SE corresponded to those reported for use of calibrated AGB maps in Section 3.3, resulting in stratum-wise RE of 0.9–2.3 for the local map and 1.0–10.4 for the global map (Table 6). The overall stratified estimates of mean AGB were 60.0 Mg ha^{-1} (SE = 2.94 Mg ha^{-1}) and 58.8 Mg ha^{-1} (SE = 2.46 Mg ha^{-1}) for the local and global maps, respectively, resulting in RE of 1.9 and 2.6, well in line with the results achieved for the global AGB maps.

Thus, the results show that even maps of attributes other than AGB can be useful for AGB estimation if properly calibrated with local plot data. Further, use of locally constructed maps with fine spatial resolution does not necessarily carry more information for precise estimation of AGB than a global map with coarser resolution.

Table 6
Estimated mean biomass (Mg ha^{-1}), systematic error (D_h; Mg ha^{-1}), standard error (SE; Mg ha^{-1}), and relative efficiency (RE) based on height maps.

			Model-assisted					
	Field-based		Biomass map produced from local height map[a]			Biomass map produced from global height map[b]		
Stratum	Mean	SE	Mean	SE	RE	Mean	SE	RE
5	44.3	4.42	42.7	3.83	1.3	39.6	3.24	1.9
6	50.4	8.39	47.4	5.51	2.3	50.7	4.87	3.0
7	81.8	10.87	100.8	8.46	1.7	87.6	7.37	2.2
8	75.4	7.50	79.4	6.42	1.4	78.1	5.26	2.0
9	37.1	12.48	37.8	12.57	1.0	50.7	3.87	10.4
12	85.1	6.71	86.0	6.98	0.9	85.4	6.61	1.0
All	57.5	4.00	60.0	2.94	1.9	58.8	2.46	2.6

[a] Trier et al. (2018).
[b] Yu et al. (2019).

3.5. Common aspects of the different analyses

All analyses indicated indifferent or positive contributions of the different maps in their original forms to increasing the precision of the various mean estimates of h_L and AGB, although the contribution was in a few cases also negative. In locally calibrated form, however, a substantial contribution of all maps to increase precision of estimates was found. Large systematic errors – positive or negative – of all maps in their original form were evident. In particular, the latter finding is somewhat disconcerting for operational application of the maps, such as for international reporting purposes. Large systematic errors would be inconsistent with the IPCC guidelines. In many tropical regions probabilistic field sample surveys are rare, expensive or infeasible due to large areas of inaccessible land for logistic or safety reasons. For these reasons, recent efforts have been devoted to the development of methods and procedures to circumvent the need for probabilistic sample surveys for ensuring compliance with the IPCC guidelines. McRoberts et al. (2019a) elaborated on various alternatives to use local maps of greater quality as means to provide a substitute for the reference data in the assessment of a map-based estimate's compliance with the non-systematic error requirement of IPCC. The assumption underpinning any assessment of a map-based estimate is that the estimate to which it is compared is obtained by an unbiased estimator and that the estimate preferably is expressed in probabilistic terms, i.e., that the reference estimate can be expressed in the form of a confidence interval. In this regard, the current findings are also alarming, because use of the local map did not indicate any greater quality than the global maps in terms of greater precision, and even though the height definition of the local height map differed from the definition of the target parameter (Lorey's mean height), the systematic map errors were so large (as great as 60 %) that differences in definitions hardly can explain the large discrepancies. Further, the finer spatial resolution of the local height map and also of one of the global AGB maps (the GFW map) was no guarantee of greater precision. In some tropical regions, at least in the current study site, it may be difficult to argue that a finer resolution map necessarily represents a "greater quality map".

These implications deviate from experiences made in other parts of the world. In a recent study from Minnesota, USA, McRoberts et al. (2019b) did not find any statistically significant systematic errors in a global AGB map that was validated locally. Clearly, there can be large regional differences in the quality of the global AGB maps, likely caused by factors such as the remote sensing sensors' sensitivity to AGB variation under various natural conditions, the structure and distribution of the AGB in various forests around the world, the methodology used to produce the map, and availability of training and calibration data in various forest types. This calls for systematic and coordinated efforts to validate global AGB maps in different forests prior to use in situations that may have political or financial implications.

4. Conclusions

Six main conclusions can be drawn from this study. First, both the local and global height and AGB maps had, in their original form, an indifferent or positive influence on the precision of mean h_L and mean AGB estimates when used to assist in the estimation, although there were cases where the contribution was negative. Second, when the very same maps were calibrated locally by use of local field plots, the calibrated maps contributed substantially to increasing the precision of both mean h_L and mean AGB estimates, with RE of 1.3–2.7 for the overall estimates. Third, the local map was not superior to the global map in assisting the estimation of mean h_L. In fact, the global map contributed equally or more to increasing the precision of the estimates. Fourth, the analysis demonstrated that if a map that represents another attribute than AGB, such as the canopy height maps, are properly calibrated with local AGB

data, they can provide substantial information to improve precision of AGB estimates. Fifth, the systematic map errors were large – positive or negative – for the local as well as the global maps. Sixth, a finer spatial resolution map did not warrant any additional information to be carried by the map that could help reduce the uncertainties of the estimates compared to more coarse-resolution maps. In fact, the fine-resolution local height map resulted in smaller RE than the coarse-resolution global height map, and the global fine-resolution AGB map resulted in smaller RE than the global coarse-resolution maps.

Finally, it is important to note that this study can only be viewed as a case study for a particular region of the dry tropical forests and with evaluation of five specific maps. The results can therefore hardly be generalized beyond the region and maps subject to analysis. However, the results clearly demonstrate potential strengths and weaknesses of local and global height and AGB maps, and that lack of knowledge of a particular map's properties in a certain region may lead to erroneous inference regarding height and AGB of potentially unwanted consequences for political and financial decisions. Therefore, additional studies of the global maps in other parts of the world and for other forest types are indeed needed.

Acknowledgments

The field work of this study was carried out as part of the project "Enhancing the measuring, reporting and verification (MRV) of forests in Tanzania through the application of advanced remote sensing techniques", funded by the Royal Norwegian Embassy in Tanzania as part of the Norwegian International Climate and Forest Initiative. The authors would like to acknowledge Ms. Antonia Ortmann and Ms Ulpu Mankinen of the Food and Agricultural Organization of the United Nations who produced the stratum map.

Appendix A

.

Table A1
Regression models for local calibration of height maps, biomass maps and biomass maps produced from height maps.

Stratum	Model	R^2	RMSE	*p*-value model[a]
Local height map (Eq. 11)				
5	$h_L = 8.385^{***} + 0.4176H^{*}$	0.04	3.22	0.028
6	$h_L = 6.112^{***} + 0.5730H^{***}$	0.10	3.91	< 0.001
7	$h_L = 7.334^{***} + 0.868H^{***}$	0.21	3.39	< 0.001
8	$h_L = 6.668^{***} + 0.6631H^{***}$	0.11	3.60	< 0.001
9	$h_L = 9.393^{**} + 0.0223H^{ns}$	<0.01	3.49	0.979
12	$h_L = 13.72^{***} - 0.2978H^{ns}$	0.03	2.64	0.280
Global height map (Eq. 11)				
5	$h_L = 8.312^{***} + 0.3073H^{***}$	0.11	3.10	< 0.001
6	$h_L = 7.513^{***} + 0.2286H^{***}$	0.10	3.92	< 0.001
7	$h_L = 9.068^{***} + 0.2916H^{***}$	0.12	3.58	< 0.001
8	$h_L = 6.767^{***} + 0.3821H^{***}$	0.17	3.48	< 0.001
9	$h_L = 6.928^{***} + 0.8935H^{*}$	0.20	3.11	< 0.001
12	$h_L = 15.83^{***} - 0.3486H^{ns}$	0.09	2.56	0.070
GFW biomass map (Eq. 12)				
5	$AGB = 23.46^{**} + 0.3085AGB_{map}{}^{**}$	0.07	29.4	0.027
6	$AGB = -4.059^{ns} + 0.6519AGB_{map}{}^{***}$	0.42	33.3	< 0.001
7	$AGB = -22.14^{ns} + 1.1019AGB_{map}{}^{***}$	0.38	49.7	< 0.001
8	$AGB = 29.00^{*} + 0.4421AGB_{map}{}^{***}$	0.09	52.7	< 0.001
9	$AGB = 10.36^{ns} + 0.4268AGB_{map}{}^{ns}$	0.05	35.5	0.318
12	$AGB = 73.33^{*} + 0.0961AGB_{map}{}^{ns}$	<0.01	36.0	0.640
GlobBiomass map (Eq. 12)				
5	$AGB = 21.23^{**} + 0.7431AGB_{map}{}^{***}$	0.21	27.1	< 0.001
6	$AGB = 14.64^{**} + 0.9471AGB_{map}{}^{***}$	0.37	34.8	< 0.001
7	$AGB = 9.781^{ns} + 1.3664AGB_{map}{}^{***}$	0.31	52.4	< 0.001
8	$AGB = 11.72^{ns} + 1.1083AGB_{map}{}^{***}$	0.16	50.5	< 0.001

(*continued on next page*)

Table A1 (*continued*)

Stratum	Model	R^2	RMSE	*p*-value model[a]
9	$AGB = 3.832^{ns} + 1.8524AGB_{map}{}^{**}$	0.37	28.9	0.002
12	$AGB = 84.19^{*} + 0.0153AGB_{map}{}^{ns}$	<0.01	36.1	0.978
JPL biomass map (Eq. 12)				
5	$AGB = 26.59^{***} + 0.3333AGB_{map}{}^{***}$	0.15	28.3	< 0.001
6	$AGB = 19.75^{***} + 0.4302AGB_{map}{}^{***}$	0.31	36.2	< 0.001
7	$AGB = 22.14^{ns} + 0.7195AGB_{map}{}^{***}$	0.28	53.3	< 0.001
8	$AGB = 28.51^{*} + 0.4500AGB_{map}{}^{***}$	0.13	51.5	< 0.001
9	$AGB = 12.91^{ns} + 1.1136AGB_{map}{}^{*}$	0.21	32.3	0.025
12	$AGB = 77.47^{*} + 0.0640AGB_{map}{}^{ns}$	<0.01	36.1	0.799
Biomass map produced from local height map (Eq. 13)				
5	$AGB = 16.80^{*} + 6.266H^{***}$	0.10	28.9	< 0.001
6	$AGB = -14.06^{ns} + 11.54H^{***}$	0.35	35.1	< 0.001
7	$AGB = -8.000^{ns} + 17.86H^{***}$	0.33	51.7	< 0.001
8	$AGB = 9.847^{ns} + 9.976H^{***}$	0.12	51.6	< 0.001
9	$AGB = 12.19^{ns} + 6.536H^{ns}$	0.02	35.9	0.463
12	$AGB = 57.18^{ns} + 3.5919H^{ns}$	0.03	35.6	0.334
Biomass map produced from global height map (Eq. 13)				
5	$AGB = 22.63^{***} + 3.494H^{***}$	0.16	28.0	< 0.001
6	$AGB = 16.25^{**} + 16.25H^{***}$	0.30	36.4	< 0.001
7	$AGB = 14.89^{ns} + 7.415H^{***}$	0.28	53.5	< 0.001
8	$AGB = 24.27^{ns} + 4.589H^{***}$	0.12	51.8	< 0.001
9	$AGB = 9.806^{ns} + 9.549H^{*}$	0.22	32.2	0.022
12	$AGB = 74.36^{*} + 0.8494H^{ns}$	<0.01	36.0	0.748

h_L: Lorey's mean height (m); H: height from map (m); AGB: aboveground biomass (Mg ha^{-1}); AGB_{map}: aboveground biomass from map (Mg ha^{-1}).
Level of significance: ns: not significant ($p > 0.05$); *: $p < 0.05$; **: $p < 0.01$; ***: $p < 0.001$.

[a] Extra sum of squares *F*-test.

References

Abdallah, J.M., Monela, G.G., 2007. Overview of miombo woodlands in Tanzania. In: In: Varmola, M., Valkonen, S., Tapaninen, S. (Eds.), MITMIOMBO – Management of Indigenous Tree Species for Ecosystem Restoration and Wood Production in Semi-Arid Miombo Woodlands in Eastern Africa. Proceedings of the First MITMIOMBO Project Workshop 50. Working Papers of the Finnish Forest Research Institute, Morogoro, Tanzania, pp. 9–23 6–12 February.

Anon, 1998. National Forest Policy. Forestry and Beekeeping Division, Ministry of Natural Resources and Tourism, United Republic of Tanzania, Dar es Salaam, pp. 59.

Anon, 2016. Emission Reductions Program Document (ER-PD). Mai-Ndombe Emission Reductions Program, Democratic Republic of Congo, pp. 295.Last Accessed May 2019. https://www.forestcarbonpartnership.org/sites/fcp/files/2016/Dec/20161108%20Revised%20ERPD_DRC.pdf.

Baccini, A., Goetz, S.J., Walker, W.S., Laporte, N.T., Sun, M., et al., 2012. Estimated carbon dioxide emissions from tropical deforestation improved by carbon-density maps. Nat. Clim. Chang. 2, 182–185.

Carreiras, J.M.B., Melo, J.B., Vasconcelos, M.J., 2013. Estimating the above-ground biomass in miombo savanna woodlands (Mozambique, East Africa) using L-band synthetic aperture radar data. Remote Sens. 5, 1524–1548.

Egberth, M., Nyberg, G., Næsset, E., Gobakken, T., Mauya, E., Malimbwi, R., Katani, J., Chamuya, N., Bulenga, G., Olsson, H., 2017. Combining airborne laser scanning and Landsat data for statistical modeling of soil carbon and tree biomass in Tanzanian Miombo woodlands. Carbon Balance Manage 12, 8. https://doi.org/10.1186/s13021-017-0076-y.

Ene, L.T., Næsset, E., Gobakken, T., Mauya, E.W., Bollandsås, O.M., Gregoire, T.G., Ståhl, G., Zahabu, E., 2016. Large-scale estimation of aboveground biomass in miombo woodlands using airborne laser scanning and national forest inventory data. Remote Sens. Environ. 186, 626–636.

Ene, L.T., Næsset, E., Gobakken, T., Bollandsås, O.M., Mauya, E.W., Zahabu, E., 2017. Large-scale estimation of change in aboveground biomass in miombo woodlands using laser scanning and national forest inventory data. Remote Sens. Environ. 188, 106–117.

Ferraz, A., Saatchi, S., Xu, L., Hagen, S., Chave, J., Yu, Y., et al., 2018. Carbon storage potential in degraded forests of Kalimantan, Indonesia. Environ. Res. Lett. 13 (9), 095001.

Frost, P., 1996. The ecology of miombo woodlands. In: Campbell, B.M. (Ed.), The Miombo in Transition: Woodlands and Welfare in Africa. Center for International Forestry Research, Bogor, Indonesia, pp. 11–57.

GFOI, 2016. Integration of remote-sensing and ground-based observations for estimation of emissions and removals of greenhouse gases in forests. Methods and Guidance From the Global Forest Observations Initiative, 2nd ed. Food and Agriculture Organization, Rome, pp. 228.Last Accessed April 2019. https://www.reddcompass.org/download-the-mgd.

GFW, 2019. Global Forest Watch Open Data Portal. https://data.globalforestwatch.org.

Gizachew, B., Solberg, S., Næsset, E., Gobakken, T., Bollandsås, O.M., Breidenbach, J., Zahabu, E., Mauya, E.W., 2016. Mapping and estimating the total living biomass and carbon in low-biomass woodlands using Landsat 8 CDR data. Carbon Balance Manage 11, 13. https://doi.org/10.1186/s13021-016-0055-8.

Globbiomass, 2019. GlobBiomass Data Portal. http://globbiomass.org/products/global-mapping.

Hansen, M.C., Potapov, P.V., Moore, R., Hancher, M., Turubanova, S.A., Tyukavina, A., et al., 2013. High-resolution global maps of 21st-century forest cover change. Science 342, 850–853.

Harris, N.L., Brown, S., Hagen, S.C., Saatchi, S.S., Petrova, S., et al., 2012. Baseline map of carbon emissions from deforestation in tropical regions. Science 336, 1573–1575.

Herold, M., Skutsch, M., 2011. Monitoring, reporting and verification for national REDD + programmes: two proposals. Environ. Res. Lett. 6, 014002.

Hojas Gascón, L., Ceccherini, G., Haro, F.J.G., Avitabile, V., Eva, H., 2019. The potential of high resolution (5 m) RapidEye optical data to estimate above ground biomass at the national level over Tanzania. Forests 10, 107. https://doi.org/10.3390/f10020107.

IPCC, 2019. Chapter 2: generic methodologies applicable to multiple land-use categories. 2019 Refinement to the 2006 IPCC Guidelines for National Greenhouse Gas Inventories Volume 4Last accessed August 2019. https://www.ipcc-nggip.iges.or.jp/

public/2019rf/index.html.
Joseph, S., Herold, M., Sunderlin, W.D., Verchot, L.V., 2013. REDD+ readiness: early insights on monitoring, reporting and verification systems of project developers. Environ. Res. Lett. 8, 034038.
Lohr, S., 1999. Sampling: Design and Analysis. Duxbury Press, pp. 494.
Lucas, R.M., Lee, A.C., Bunting, P.J., 2008. Retrieving forest biomass through integration of CASI and LiDAR data. Int. J. Remote Sens. 29, 1553–1577.
Mauya, E.W., Ene, L.T., Bollandsås, O.M., Gobakken, T., Næsset, E., Malimbwi, R.E., Zahabu, E., 2015. Modelling aboveground forest biomass using airborne laser scanner data in the miombo woodlands of Tanzania. Carbon Balance Manag. 10, 28. https://doi.org/10.1186/s13021-015-0037-2.
McRoberts, R.E., Vibrans, A.C., Sannier, C., Næsset, E., Hansen, M.C., Walters, B.F., Lingner, D.V., 2016. Methods for evaluating the utilities of local and global maps for increasing the precision of estimates of subtropical forest area. Can. J. For. Res. 46, 924–932.
McRoberts, R.E., Næsset, E., Liknes, G.C., Chen, Q., Walters, B.F., Saatchi, S., Herold, M., 2019a. Using a finer resolution biomass map to assess the accuracy of a regional map-based estimate of forest biomass. Surv. Geophys. 15. https://doi.org/10.1007/s10712-019-09507-1.
McRoberts, R.E., Næsset, E., Saatchi, S., Liknes, G.C., Walters, B.F., Chen, Q., 2019b. Local validation of global biomass map. Int. J. Appl. Earth Obs. Geoinf. https://doi.org/10.1016/j.jag.2019.101931.
Mitchard, E.T.A., Saatchi, S.S., Lewis, S.L., Feldpausch, T.R., Woodhouse, I.H., Sonké, B., Rowland, C., Meir, P., 2011. Measuring biomass changes due to woody encroachment and deforestation/degradation in a forest–savanna boundary region of central Africa using multi-temporal L-band radar backscatter. Remote Sens. Environ. 115, 2861–2873.
Mitchard, E.T.A., Saatchi, S.S., Baccini, A., Asner, G.P., Goetz, S.J., Harris, N.L., Brown, S., 2013. Uncertainty in the spatial distribution of tropical forest biomass: a comparison of pan-tropical maps. Carbon Balance Manag. 8 (1), 10.
MNRT, 2015. National Forest Resources Monitoring and Assessment (NAFORMA) Main Results. Tanzania Forest Services, Ministry of Natural Resources and Tourism, Dar es Salaam, Tanzania, pp. 106.
Mugasha, W.A., Eid, T., Bollandsås, O.M., Malimbwi, R.E., Chamshama, S.A.O., Zahabu, E., Katani, J.Z., 2013. Allometric models for prediction of above- and belowground biomass of trees in the miombo woodlands of Tanzania. For. Ecol. Manage. 310, 87–101.
Næsset, E., Bollandsås, O.M., Gobakken, T., Solberg, S., McRoberts, R.E., 2015. The effects of field plot size on model-assisted estimation of aboveground biomass change using multitemporal interferometric SAR and airborne laser scanning data. Remote Sens. Environ. 168, 252–264.
Næsset, E., Ørka, H.O., Solberg, S., Bollandsås, O.M., Hansen, E.H., Mauya, E., Zahabu, E., Malimbwi, R., Chamuya, N., Olsson, H., Gobakken, T., 2016. Mapping and estimating forest area and aboveground biomass in miombo woodlands in Tanzania using data from airborne laser scanning, TanDEM-X, RapidEye, and global forest maps as auxiliary information: a comparison of estimated precision. Remote Sens. Environ. 175, 282–306.
Naidoo, L., Cho, M.A., Mathieu, R., Asner, G., 2012. Classification of savanna tree species, in the Greater Kruger National Park region, by integrating hyperspectral and LiDAR data in a Random Forest data mining environment. Isprs J. Photogramm. Remote. Sens. 69, 167–179.
Good practice guidance for land use, land-use change and forestry. In: Penman, J., Gytarsky, M., Hiraishi, T., Krug, T., Kruger, D., Pipatti, R., Buendia, L., Miwa, K., Ngara, T., Tanabe, K., Wagner, F. (Eds.), Intergovernmental Panel on Climate Change. Institute for Global Environmental Strategies, Hayama, Japan.
Quegan, S., Rauste, Y., Bouvet, A., Carreiras, J., Cartus, O., Carvalhais, N., LeToan, T., Mermoz, S., Santoro, M., 2017. DUE GlobBiomass. D6 – Global Biomass MapAlgorithm Theoretical Basis Document. Prepared for European Space Agency (ESA-ESRIN). In response to ESRIN/Contract No. 4000113100/14/I_NB, 137 pp. Available at: http://dropbox.gamma-rs.ch/fe4ab363-3d65-4dc8-8d3c-fc7fbc2a9afa/GlobBiomass_D6_7_Global_ATBD_final.pdf. (last accessed: May 2019).
Saatchi, S.S., Harris, N.L., Brown, S., Lefsky, M., Mitchard, E.T.A., et al., 2011. Benchmark map of forest carbon stocks in tropical regions across three continents. Proceedings of the National Academy of Sciences, U.S.A 108, 9899–9904.
Santoro, M., Cartus, O., Mermoz, S., Bouvet, A., Le Toan, T., Carvalhais, N., Rozendaal, D., Herold, M., Avitabile, V., Quegan, S., Carreiras, J., Rauste, Y., Balzter, H., Schmullius, C., Seifert, F.M., 2018. A detailed portrait of the forest aboveground biomass pool for the year 2010 obtained from multiple remote sensing observations. Geophysical Research Abstracts 20, EGU2018–18932 EGU General Assembly 2018.
Särndal, C.-E., 1984. Design-consistent versus model-dependent estimation for small domains. J. Am. Stat. Assoc. 79, 624–631.
Särndal, C.-E., 2011. Combined inference in survey sampling. Pak. J. Stat. Oper. Res. 27, 359–370.
Särndal, C.-E., Swensson, B., Wretman, J., 1992. Model Assisted Survey Sampling. Springer-Verlag, Inc., New York, pp. 694.
Shimada, M., Itoh, T., Motooka, T., Watanabe, M., Shiraishi, T., Thapa, R., Lucas, R., 2014. New global forest/non-forest maps from ALOS PALSAR data (2007–2010). Remote Sens. Environ. 155, 13–31.
Tomppo, E., Malimbwi, R., Katila, M., Mäkisara, K., Henttonen, H.M., Chamuya, N., Zahabu, E., Otieno, J., 2014. A sampling design for a large area forest inventory: case Tanzania. Can. J. Res. 44, 931–948.
Trier, Ø.D., Salberg, A.-B., Haarpaintner, J., Aarsten, D., Gobakken, T., Næsset, E., 2018. Multi-sensor forest vegetation height mapping methods for Tanzania. Eur. J. Remote. Sens. 51, 587–606.
URT, 2010. National Forestry Resource Monitoring and Assessment of Tanzania (NAFORMA). Field Manual. Biophysical Survey. Ministry of Natural Resources & Tourism, The United Republic of Tanzania, Dar es Salaam, pp. 95 Available at: http://www.fao.org/forestry/23484-05b4a32815ecc769685b21b03be44ea77.pdf. (last accessed: May 2018).
White, F., 1983. The Vegetation of Africa, a Descriptive Memoir to Accompany the UNESCO/AETFAT/UNSO Vegetation Map of Africa (3 Plates, Northwestern Africa, Northeastern Africa, and Southern Africa, 1: 5,000,000). United Nations Educational, Scientific and Cultural Organization, Paris, France.
Xu, L., Saatchi, S.S., Yang, Y., Yu, Y., White, L., 2016. Performance of non-parametric algorithms for spatial mapping of tropical forest structure. Carbon Balance Manag. 11 (1), 18.
Xu, L., Saatchi, S.S., Shapiro, A., Meyer, V., Ferraz, A., Yang, Y., et al., 2017. Spatial distribution of carbon stored in forests of the Democratic Republic of Congo. Sci. Rep. 7 (1), 15030.
Yu, Y., Saatchi, S., Yang, Y., Xu, L., Meyer, V., Longo, M., et al., 2019. Diversity of structure and carbon density of wood vegetation of the Earth. Under Review in Science Advances.